Integration of ARGO trajectories in the Mediterranean Forecasting System and impact on the regional analysis of the Western Mediterranean circulation

by

V. Taillandier[1], S. Dobricic[2], P. Testor[3], N. Pinardi[4], A. Griffa[5, 6], L. Mortier[3], G.P. Gasparini[5]

[1] LOV, Villefranche-sur-Mer, France

[2] CMCC, Bologna, Italy

[3] LOCEAN-IPSL, Paris, France

[4] INGV, Bologna, Italy

[5] CNR-ISMAR, La Spezia, Italy

[6] RSMAS, University of Miami, Florida, USA

submitted to

Journal of Geophysical Research

December 19, 2008

corresponding author:

Vincent Taillandier, LOV-CNRS, BP08, 06230 Villefranche-sur-Mer, France

tel: +33 4 93 76 37 36; e-mail: taillandier@obs-vlfr.fr

Abstract

The impact of ARGO trajectory assimilation on the quality of ocean analyses is studied by means of an operational oceanographic model implemented in the Mediterranean Sea and a 3D-var assimilation scheme. For the first time, both ARGO trajectories and vertical profiles together with satellite data are assimilated to produce analyses for short term forecasts. The study period covers three months during winter 2005 when four ARGO trajectories were present in the northwestern Mediterranean Sea. It is shown that their integration is consistent with the other components of the assimilation system, and it contributes to refine the model error structure with new information on horizontal pressure gradients. So the analysis benefits of a more accurate description of the boundary currents and their instabilities that drive the mesoscale activity of regional circulations. As a consequence, the trajectory assimilation remotely and significantly influences the basin scale circulation. Changes can be depicted by intermediate water mass redistributions, mesoscale eddy relocations or net transports modulations. These impacts are detailed and assessed considering historical and contemporary datasets. The obtained qualitative and quantitative agreements motivate the integration of ARGO trajectories in the operational Mediterranean Forecasting System.

1. Introduction

In a regional sea like the Mediterranean, the basin scale circulation is strongly influenced by mesoscale features. They are triggered by vertical mixing or baroclinic instability (Crépon et al., 1982), generating eddies (up to ~100km of diameter) whose lifetime can span several months or even years (Puillat et al., 2002; Taupier-Letage et al., 2003). These mesoscale features significantly influence momentum and thermohaline fluxes. The large eddies can strongly perturb and in some cases even block the large scale circulation (Bouzinac et al., 1999; Testor et al., 2005a). The smaller eddies (~10-20km of diameter) contribute significantly to the formation and spreading of dense waters by acting on dispersion and on lateral mixing (Madec et al., 1996; Testor and Gascard, 2006; Demirov and Pinardi, 2007). At the shelf interface, they can influence the renewal of coastal waters through the regulation of offshore exchanges (e.g., Mariano et al., 2003).

For these reasons, observations and models that both resolve the mesoscale variability need to be considered together, in order to provide best estimates and forecasts of the Mediterranean circulation. That is why the Mediterranean Forecasting System (hereafter MFS) has been developing the observational and modeling bases for the estimation of the circulation at the basin scale with mesoscale resolution (Pinardi et al., 2003). Observing systems have been designed for a routine and automated monitoring of the mesoscale at the level of the major Mediterranean sub-basins. The monitoring is realized in first instance by satellite altimeters (Le Traon et al., 2003) and radiometers (Buongiorno Nardelli et al., 2003; Marullo et al., 2007). In-situ observing efforts have been concentrated on Ship of Opportunity Programs (Manzella et al., 2007), surface drifters and autonomous profilers (Poulain et al., 2007), mooring networks (Nittis et al., 2007), and glider sections (Dobricic et al., in revision). On the other hand, circulation models have been upgraded in order to fully resolve the mesoscale dynamics (Béranger et al., 2005; Tonani et al., 2008). Assimilation techniques have also been upgraded in order to provide multivariate analysis of the ocean circulation (Dobricic et al., 2005, 2007) permitting enhanced dynamical constraints (Dobricic and Pinardi, 2008).

Thanks to these developments, the MFS nowadays assimilates two satellite altimeters along track data, satellite daily sea surface temperature, and vertical hydrological profiles of Temperature (T) and Salinity (S) from XBT and ARGO profilers. ARGO float trajectories have not been integrated yet, even though they contain direct information on ocean currents in the open sea as well as near the shelf. Assimilating trajectory data is challenging for a number of reasons, both theoretical and practical (Kamachi and O'Brien, 1995; Ishikawa et al., 1996; Ozgokmen et al., 2000; Ide et al., 2002), and suitable methodologies have been developed only in the last few years (Molcard et al., 2003, 2005; Kuznestov et al. 2003; Taillandier et al., 2006a, Nodet, 2006). From the theoretical point of view, the issue of the non-linear relationship between float position data, that describe the subsurface drift between two profiles, and the ocean current estimates have been addressed (Taillandier et al., 2006a). From the more practical point of view, specific sampling issues related to ARGO trajectories have been investigated using the OSSE (Observing System Simulation Experiment) approach with virtual floats (Taillandier and Griffa, 2006). In particular, the fact that ocean currents are measured rather sparsely with a trajectory sampling of some days, and rather noisily due to the non-measurable shear drifts experienced during the profiling sequences have been considered. Based on these preliminary investigations, a first test of assimilation of the in-situ ARGO trajectories in isolation in a Mediterranean Sea model has been performed (Taillandier et al., 2006b), and it showed the non negligible impact of the assimilation with significant changes in the ocean circulation.

In this paper, we address a similar assessment for ARGO trajectory assimilation, but this time, in the frame of an operational forecasting system such as MFS. Differently from the previous studies where only trajectory assimilation was considered (Taillandier et al., 2006a,b), here trajectory data are considered together with the other data of the MFS observation system, i.e. sea surface topography and TS profiles. This is an important step for potential improvement of operational predictive systems, given that ARGO floats are an integral and fundamental part of the observing system over the whole ocean and the full exploitation of their information is expected to of great benefit. Trajectories data are quasi-Lagrangian, i.e. they follow with some approximation the ocean currents, so that their information is directly related to drift velocity. Assimilating them is a potentially powerful information to improve prediction, but at the same time their compatibility with the other data and with the model itself must be carefully tested.

The present study has three main goals:

- To introduce the assimilation technique that has been developed for the multivariate assimilation of the MFS system including the ARGO trajectories, and that will be used in operational mode.
- To verify that the trajectory assimilation is consistent with the assimilation of the other mass data and with the model mass variables.
- To investigate the specific impact of trajectory assimilation on the various processes and scales of the MFS prediction system.

In order to implement the combined assimilation of altimeters, trajectory and profile data, we take benefit from the new formulation of the MFS assimilation scheme that has recently been upgraded to a 3D-var scheme (Dobricic and Pinardi, 2008). A new observation operator is added to the procedure, using a well tested scheme for Lagrangian data analysis (Taillandier et al., 2006a, Taillandier et al., 2008).

The performance of the system is tested considering the same region and period previously considered by Taillandier et al. (2006b) that assimilated trajectories in isolation. The choice is primarily dictated by the satisfactory data coverage, consisting in four floats in the region during three months. In addition to this, the choice also allows for a qualitative comparison with the results of Taillandier et al (2006b) providing indirect information on the impact of the MFS observing system (that was not included in this previous study). The analysis is performed, and several sensitivity diagnostics on the Mediterranean circulation are provided, considering or not the assimilation of ARGO trajectories.

As a first step, the question of internal consistency is considered by testing whether or not the trajectory assimilation alters the misfits with respect to the model variables. This is a relevant and non-trivial question. Given the great number of scales and processes present in the ocean, data compatibility is not always guaranteed, especially for drift related quantities that sample all the scales of motion and are directly affected by ageostrophic processes. Indeed, the issue of "representativeness", i.e. the impact of spatial and temporal variability of the measured quantities with respect to the scales of the analysis, is one of the great challenges faced by operational oceanography. The results of the present analysis will provide a first assessment for the ARGO trajectories.

The other assessments, including hydrological sections, transport, mean circulation and variability, are aimed at quantifying the impact of trajectory assimilation, trying to identify which processes and scales are mostly influenced. Given the reduced number of independent data available in the considered period, most of the analysis is performed comparing results obtained with and without trajectory assimilation, and considering a qualitative match with respect to historical data. This provides a first insight on the new skills for model predictability and helps identifying the circulation features and the motion scales whose corrections are more effective when assimilating also ARGO trajectories.

Finally a comparison is performed with the only set of independent in-situ data available for comparison in the period of interest: transport data from current meters in the Corsica Channel (Astraldi et al., 1999). They have been previously used in Taillandier et al. (2006b), and they are considered here, comparing them with estimates obtained with and without trajectory assimilation. The Corsica Channel is not directly sampled by the floats, but the estimates of transport appear influenced by the presence of nearby trajectories, therefore providing an interesting first quantitative indication on the skills of trajectory assimilation.

The paper is organized as follows. Section 2 describes the integration of ARGO trajectories in the MFS assimilation scheme and its expected impact on the model error structure. Section 3 deals with the experimental set up while the results are presented in Section 4. Summary and concluding remarks are drawn in Section 5.

2. Method

The integration of ARGO trajectories in the MFS assimilation scheme has been preliminarily investigated in isolation (i.e. assimilating the trajectory data alone) and assessed using a “twin experiment” approach reported in Taillandier and Griffa (2006). The next methodological step considered in the present paper is to effectively consider ARGO trajectories together with the other data information included in the MFS observation system, i.e. Sea Level Anomalies (hereafter SLA) and Sea Surface Temperature (SST) data from satellites, and vertical TS profiles from XBT and ARGO floats. This is done using a 3D-var scheme recently developed (Dobricic and Pinardi, 2008).

a) Integration of ARGO trajectories in the assimilation scheme

The principle of the 3D-var approach is to find iteratively the minimum of the cost function J:

$$J = (x - x^{bck})^T . \mathbf{B}^{-1} . (x - x^{bck}) + (\boldsymbol{H}(x) - y)^T . \mathbf{R}^{-1} . (\boldsymbol{H}(x) - y) \qquad (1)$$

where x is the model state vector, x^{bck} is its background or first guess, y the observation vector, $\boldsymbol{H}$ the observation operator, **B** and **R** the error covariance matrices for x^{bck} and y respectively. The model state variables contained in x are temperature T, salinity S, velocity components **u** and sea level η.

In this formalism, the integration of ARGO trajectory observations consists in extending the observation vector y with the positions $\mathbf{r}^{obs}$ acquired at each time t_n when the profilers surface. Then the minimization of J at time t_n requires also the model equivalent **r** for float positions. This new quantity is computed by integrating the particle advection equation during the previous surfacing time t_b and the present one t_n:

$$d\mathbf{r} / dt = \mathbf{u}(\mathbf{r}(t), t),\ t \in [t_b, t_n] \quad \text{with } \mathbf{r}(t_b) = \mathbf{r}^{obs}(t_b) \tag{2}$$

This trajectory description is effectively implemented in the 3D-var scheme as a new component of the observation operator $\boldsymbol{H}(x)$. Note that according to the ARGO cycle, the 4D structure of the model state is involved in Eq.(2). The time-varying velocity field **u** is required at the float parking depth during the whole subsurface drift, but also along the vertical to account for shear drift experienced during dives at t_b and surfaces at t_n. In numerical practice, the trajectory computation of each ARGO float is included in the model simulation, starting from the last observed position ($\mathbf{r}^{obs}(t_b)$ in Eq.(2)), and it is updated with the new observed positions ($\mathbf{r}^{obs}(t_n)$) when the minimization of J is achieved.

Coming back to the description of the 3D-var scheme, the corrected model field, or analysis field, can be written in the form:

$$x = x^{bck} + \mathbf{V}.v \tag{3}$$

where v is the so-called control vector and its error covariance matrix **V** built such as $\mathbf{B} = \mathbf{V}.\mathbf{V}^T$. The cost function in Eq.(1) is linearized around x^{bck} and it is re-written in terms of the control vector v such as

$$\delta J = v^T.v + (\ \mathbf{H}.\mathbf{V}.v - d\ )^T.\ \mathbf{R}^{-1}.\ (\ \mathbf{H}.\mathbf{V}.v - d\ ) \tag{4}$$

where d is the innovation vector measuring the misfit between the observation vector y and its modeled first guess $\boldsymbol{H}(x^{bck})$, and **H** is the linearized observation operator.

In this formalism, the float position data are included in the innovation vector d at each time t_n they are available. The innovation associated to trajectories is computed as the misfit between the observed positions $\mathbf{r}^{obs}(t_n)$ and the positions $\mathbf{r}^{bck}(t_n)$ simulated inside the background velocity field (Eq.(2)). Then, the minimization of δJ (Eq.(4)) requires an increment for float positions, linearly expressed from the control vector v (Eq.(3)) by the observation operator **H**. This new quantity is computed by integrating a linearized version of the particle advection equation (Eq.(2)) around the background velocity field. The expression of this position increment has been discussed in Taillandier et al. (2006a), and the proposed formulation has been taken up to build **H** and $\mathbf{H}^T$. Overall, the minimization of δJ when fitting position data provides sequential velocity corrections which are used to re-initialize the circulation model at the end of float drifts (Eq.(2)). They represent time-independent (during the observation interval) subsurface structures that identify the observed drifts (with respect to Eq.(2)) when superimposed to the background velocity field.

b) Heterogeneous observing system

The Mediterranean observing system assimilated in the MFS is composed of data routinely acquired by three types of instrumentations. The ARGO profilers sample the stratification of the water column and return their subsurface drift positions every 5 days (Poulain et al., 2007). The ARGO trajectories are used to document the ocean current at the float parking depth of 350m. The XBTs instead sample the potential temperature along tracks with high spatial resolution but at coarser time resolution (Manzella et al., 2007). The satellite altimeters sample SLA along tracks with a synoptic coverage and a large periodicity (Le Traon et al., 2003), they provide information on sea surface topography. So the considered datasets are highly heterogeneous in nature and spatio-temporal distribution. Moreover, they are assimilated sequentially in order to re-initialize the circulation model from a daily analysis. Let us detail the respective contributions of altimeters SLA, TS profiles and subsurface trajectories (at 350m depth) in the assimilation procedure.

The observations are used by the 3D-var scheme in order to compute the optimal correction of the background model state x^{bck}. As already seen with Eq.(3), this optimization problem is reduced to the estimation of a set of control parameters (vector v). The transformation of the control vector into "physical" model variables is defined by the background error covariances (matrix **V**). Dobricic and Pinardi (2008) detailed the construction of this **V** that is modeled by a sequence of linear operators such as

$$\mathbf{V} = \mathbf{V}_{uv}.\ \mathbf{V}_{\eta}.\ \mathbf{V}_{H}.\ \mathbf{V}_{V} \qquad (5)$$

$\mathbf{V}_V$ transforms weighting coefficients (control vector v) which multiply vertical EOFs into vertical profiles of temperature and salinity corrections. $\mathbf{V}_H$ applies horizontal covariances of temperature and salinity using a recursive filter that models an isotropic Gaussian correlation pattern for the two passive tracers. $\mathbf{V}_\eta$ estimates the corrections of the sea surface height using a barotropic model forced by the corresponding density perturbations and topography. $\mathbf{V}_{uv}$ estimates the baroclinic part of the velocity correction in geostrophic balance with the surface pressure gradient (from sea surface height correction) and hydrostatic pressure gradient (from density correction).

The adjoint of Eq.(5) transforms the contribution of each observations, into a measure of their sensitivity (in terms of optimal step toward the best linear estimate). In particular, the contribution of ARGO trajectories is projected on the model velocity through $\mathbf{V}_{uv}^T$. It impacts on hydrostatic pressure gradients thanks to $\mathbf{V}_{uv}^T$, on the model sea level thanks to $\mathbf{V}_\eta^T$, and finally it changes the horizontal and vertical structure of the mass field thanks to $(\mathbf{V}_H.\mathbf{V}_V)^T$.

Such insight appears particularly interesting given that ARGO floats provide simultaneously one hydrological profile and one subsurface drift. Hence, these two contributions would document the stratification of the water column at the location of the profile, together with the horizontal gradients of this stratification in the normal direction of the drift at the float parking depth. As a first consequence, the horizontal structure of the model error would not be isotropic anymore, but shaped as a combination of the “dipolar” correction pattern of horizontal gradients on T and S, with a “circular” (isotropic) correction pattern of T and S. As a second consequence, the vertical structure of the TS profiles will extend this complex horizontal pattern on the vertical direction, thus correcting the vertical shear of the geostrophic currents. This effect is now to be assessed in the following numerical framework.

3. Experimental set up

a) Two analyses of the Mediterranean circulation

The results reported in the present study focus on the comparison between two analyses of the Mediterranean circulation, focused on the western basin (Figure 1). The first analysis called “OSref” uses assimilation of observations of SLA and TS profiles, while the second analysis called “OStrj” uses also the trajectory data in addition to the SLA and TS observations. The 3D-var assimilation scheme described in Dobricic and Pinardi (2008) is used to perform the analysis OSref. The same scheme with the additions detailed in Section 2a is used to perform the analysis OStrj.

The two assimilation experiments start from the same initial state, corresponding to the analysis OSref for January 1, 2005 and last the following 3 months (January 1 – March 31, 2005) in order to cover the whole wintertime period. At the initial time of January 1 2005, OStrj will then introduce the assimilation of trajectories for this period while OSref will continue without them. The Mediterranean model configuration is the one described in Tonani et al. (2008), generated over a meshgrid of resolution 1/16 degree. Background error correlations are computed with vertical time-dependent EOFs as reported in Dobricic et al. (2007).

b) Four ARGO trajectories over the NW Mediterranean Sea

Four ARGO floats are available in the NW Mediterranean Sea during the period of interest (Poulain et al., 2007). Their trajectories (Figure 1) are indicative of the float displacements at a parking depth of 350m sampled every 5 days. The westernmost float is initially trapped inside a mesoscale eddy then it exits from this structure to drift in the so-called Balearic Current (Font et al., 1988) that flows eastward along the islands. Another float describes a circle loop in the central basin. In the easternmost area, the two other floats are observed (despite some gaps on position time series) to drift northward into the Ligurian Sea. They document the flow of the Levantine Intermediate Water (LIW) along western Sardinian and Corsican coasts (Millot, 1999). Note that the Northern Current that flows along the continental coast is not sampled by this trajectory dataset.

c) Diagnostics

Various diagnostics are performed with the aim of comparing the two analyses OSref and OStrj. They are computed from the daily mean outputs of the model state. They provide a self-consistent assessments with respect to the assimilated dataset (heterogeneous in nature and distribution). They also consider regional circulations with the goal of characterizing the impact of the trajectory assimilation on the mean and the variability of the obtained estimates.

The first diagnostic investigates the misfits between TS profiles as analyzed and as observed by the four ARGO floats. The analyzed mass field is interpolated at the time and location of each observed profile (with population of ~80 profiles during the period), and the misfit is calculated as well as its root mean square value considering all the TS data acquired by the four ARGO floats during the three-month period.

The second diagnostic considers the seasonal mean stratification and circulation over the region of interest. The mean velocity field is computed at the parking depth of the ARGO floats (350m) over the western Mediterranean and over the three month period. The choice of this depth is also motivated by a representation of the indicative flow that infers LIW pathways. This horizontal point of view is enriched in the vertical considering four relevant sections indicated in Figure 1. The salinity field and the normal component of the absolute velocity field (i.e. assembling geostrophic and ageostrophic components) are computed interpolating along the sections and averaging over the three month period.

The third diagnostic focuses on the characteristics of time variability. It includes a computation of the surface Eddy Kinetic Energy (EKE) averaged over the three month period for the two analyses OSref and OStrj. The EKE provides a measure of the amplitude of variations which characterize the time evolution of the surface flow. They are induced by assimilated SLA data in geostrophic balance with the barotropic flow, as well as by the complete model dynamics and its answer to the atmospheric forcing. The EKE computed from the analysis OSref, called

EKEref, constitutes a reference for the overall level of energy. The consistency of the analysis OStrj is then assessed computing its EKE, called EKEtrj, and focusing on the energy inputs generated by the integration of ARGO trajectories. In practice, this is done first of all by computing the following difference

$$\mathrm{EKEdiff} = \mathrm{EKEtrj} - \mathrm{EKEref} \tag{6}$$

that directly documents the changes in the spatial distribution of eddy energy. As a second step, the absolute value of EKEdiff is normalized with respect to the level of the reference as

$$\mathrm{EKEnorm} = \| \mathrm{EKEdiff} \| / \mathrm{EKEref} \tag{7}$$

in order to study the consistency of the operated changes due to trajectory integration. Note that EKref and EKEtrj are computed from surface currents analyzed by OSref and OStrj and degraded over the same 1/8° meshgrid. A spatial smoothing filter with an isotropic cut-off radius of 10km is applied to the obtained differences to remove the smallest spots and keep the most representative patterns.

d) Independent datasets

Two datasets are considered for a contemporary description of circulation features independently from the ones analyzed in OSref and OStrj. They are provided by observations routinely acquired by in-situ and remote sensing means.

Satellite altimeters allow a well-fitted description of the seasonal mean patterns of the circulation which can be reliable to one obtained by the two analyses. Note that the SLA measured by these altimeters are also assimilated to perform the analyses. Another way to exploit these observations is to reconstruct absolute geostrophic velocities which are derived from sea surface heights and estimated in gridded products (Ssalto/Duacs User Handbook, 2006). To do so, the SLA data are combined with a mean dynamic topography (Rio et al., 2007), in order to restore absolute velocities at a spatial resolution of 1/8 degree and a temporal resolution of a week. Their average over the three-month period is then computed and used in the present study to compare the location and shape of circulation structures analyzed in OSref and OStrj and described by the second diagnostic (Section 3c).

Thanks to the continuous monitoring of the exchanges across the Corsica Channel (Astraldi et al., 1999), time series of the net transport obtained by the two analyses can be quantitatively compared to contemporary and independent in-situ data. Note that at the location of the section D (indicated in Figure 1), the Corsica Channel is narrow (65km width), and mainly shallow (100m depth) except at a canyon reaching 450m at the bottom of which a current meter has been moored. Current profile data are extrapolated to provide an estimate of the net transport crossing the strait. So the measurements and the numerical estimates of the transports are definitely reliable. This comparison is achieved inside an admissible envelope built from a central value given by current meter data averaged on successive 4-day windows, and by the associated standard deviation inside these 4-day windows. On the other hand, a value of the transport integrated from surface to bottom over the section D is calculated daily from analyzed model outputs during the three-month period. A smoothing filter with a cut-off value of 4 days is applied to the analyzed time series in order to remove high frequency fluctuations.

4. Results

Considering the material and the numerical approaches exposed in the Sections 2-3, the results reported hereafter would assess the self consistency of the Mediterranean Forecasting System when assimilating ARGO trajectories, and point out the corresponding impacts on regional circulations. We will see that the trajectory assimilation yields to significant changes at mesoscale, so the realism of the obtained shifts will be checked considering eddy energy inputs and independent (historical and contemporary) datasets.

a) Self consistency

Figure 2 shows the temperature and salinity misfits for the two analyses OSref and OStrj. As it can be seen, the difference between the two analyses is very small for temperature (Figure 2a) and is negligible for salinity (Figure 2b). The difference in the temperature misfits shows that, at the position of ARGO floats, the trajectory assimilation has slightly improved the accuracy of temperature analyses above the depth of 300m and has slightly reduced it below. Overall, the trajectory assimilation does not alter the TS estimates and it actually improves them slightly in some places. This is a relevant result, because it indicates that the trajectory assimilation is consistent with the assimilation of TS profiles and with the mass variables of the model.

The trajectory assimilation is expected to provide significant corrections on the temperature and salinity gradients (thus on the hydrostatic pressure gradients) in a direction orthogonal to the subsurface drift of the floats (as discussed in Section 2b). As a consequence, differences in temperature and salinity estimates are expected to occur not only at the observation points but also (and mainly) in their neighborhood, which is now investigated.

b) Impact on the mean circulation

We consider the mean velocity field at the parking depth of the ARGO floats (350m) that is also characteristic of the LIW circulation. It is represented for the two analyses OSref and OStrj in Figure 3, together with their misfit and the mean velocity field reconstructed from sea surface topography (see Section 3d). The trajectories are superimposed to the velocity fields to facilitate the interpretation. Notice that since the velocity fields are averaged over three months, a visual close match between trajectories and currents cannot be expected, especially in areas of high variability.

The basin scale circulation in the intermediate layer appears in good agreement with the circulation schemes reported from field surveys (Millot, 1999; Testor et al., 2005b) for the two analyses. In the Provençal basin (i.e. the northern central part of the area, see Figure 1), a cyclonic circulation is developed along the continental coast from the Ligurian Sea to the Balearic Sea. The return branch meanders between (40°N, 4°E) and (41°N, 8°E) which is identified in the surface layer as the Balearic Front (e.g., Deschamps et al., 1984). In the Algerian basin (i.e. the southern part of the area, see Figure 1), well known features of the regional circulation are represented in the analyses, with a meandering current from along the continental coast (e.g. Millot, 1985) and a large anticyclonic eddy (Taupier-Letage et al., 2003) offshore the coast at (38°N, 6°E).

In this basin scale point of view, some differences appear between the two analyses (Figure 3c). We can notice that the correction patterns often shape as dipolar structures, such as the one located at (38°N, 6°E), as well as single loop structures, such as the one located at (40.5°N, 3°E). The first type of correction pattern depicts spatial shifts of eddies, instead the second type depicts modulations of boundary currents. Their distribution in Figure 3c covers the four trajectory pathways, which indicates the local impact of trajectory assimilation on the intermediate circulation. The spatial shifts are also distributed far away from trajectories, sometimes further than an internal radius (~20km), which indicate the remote impact of trajectory assimilation. For example, the daisy chain of spatial shifts crossing the Provençal basin indicates the reorganization of the eddy field in this region. Also in the Algerian basin, the relocation of the Algerian eddy (at 38°N, 6°E) is strongly marked in the Figure 3c. We will come back more precisely to these correction patterns in the following regional studies (Sections 4c-e).

In order to get the vertical dimension of such impacts and to look at their consequences in terms of water mass circulation (specially for the LIW), three sections crossed by ARGO trajectories are considered (see Figure 1). As detailed in Section 3c, the mean seasonal stratification given by isohalines is represented along these sections, while isolines of absolute normal velocities, averaged over the same three-month period, are superimposed in the Figures 4-6. The main characteristics of stratification and currents are preserved between OSref and OStrj, in agreement with what discussed in Section 4a, and further indicating the consistency of the trajectory data. Nevertheless, specific differences can be seen, especially where the floats cross the sections. The obtained features can be qualitatively compared to what is known from historical datasets in the area.

Before going to case by case investigations over three regional seas, let us look at the basin scale distribution of water masses along the section B that crosses the whole area from south to north. Shown in Figure 4, the salty Mediterranean waters contrast with the fresh waters of Atlantic origin, so they spread under the surface layer (deeper than 200m). Their properties are altered when going to the north, with a clear separation at 40.5°N. Around this interface (between 39.5°N and 41.5°N), the structure under the Balearic Front is significantly different in the two analyses. A clear cyclonic loop in OSref around the reservoir doming at 39.5°N and 300m depth (Figure 4a) is weakened in OStrj with the generation of an eastward branch at 40.2°N. So the general cyclonic pattern around the salty reservoir doming at 42°N is reinforced with trajectory assimilation. Impacts in the mesoscale activity can also be noticed along the section B. For example the deepening of the halocline at 38.4°N or the slope of the doming in the northern basin (at 42.1°N) appear clearly accentuated in OStrj. They can be linked to the spatial shift of eddies which are crossed by the section B closer to their center.

c) Case of the Balearic Sea

The differences which were quickly depicted in the previous basin scale point of view are now detailed for the Balearic Sea. The current system of this area represented in Figure 3 and crossed by the section A is composed of the Balearic Current, flowing eastward along the islands, and the Northern Current, flowing westward along the continental slope (Font et al., 1988). In effect looking at Figure 5, the two analyses OSref and OStrj provide steep isohalines in the neighborhood of the coasts, indicating the presence of two boundary currents, the Northern Current along the eastern continental coast and the Balearic Current along the western coast. Main differences can be seen in the Balearic Current as expected as the only one directly sampled by a trajectory (Figure 1). Horizontal salinity gradients at 2.9°E are stronger in OSref (Figure 5a) than in OStrj (Figure 5b). So the core of the Balearic Current appears more intense and more confined along the coast without trajectory assimilation. This is also confirmed by the shape of absolute velocities crossing the section, but not by the mean circulation reconstructed from sea surface topography (Figure 3d).

The general structure of the currents in this section is in qualitative agreement with what is known about the area (Pinot and Ganachaud, 1999; Schroeder et al., 2008), even though a quantitative assessment cannot be made, primarily due to data scarcity, but also because of the very high variability, especially concerning the structure and the intensity of the Northern Current (La Violette et al., 1990; Pinot et al., 2002). Historical springtime field survey measurements by Pinot and Ganachaud (1999) show patterns that are qualitatively similar to the ones in both analyses, while results by Schroeder et al. (2008), taken in April-May 2005 i.e. a few months later than the present analysis, indicate a less intense and less deep current. Note that features of flow reversal has been extensively reported and related to seasonal and mesoscale variability (Pinot et al., 2002; Pascual et al., 2002). So the correction in OStrj also goes in the direction of weakening the Balearic Current, even though significantly less than it is in Schroeder et al. (2008).

As an interesting side note, we point out that the current along the Balearic Islands was absent in the free (i.e. without assimilation) model run considered in Taillandier et al. (2006b), and it was introduced solely by the trajectory assimilation (see Figure 3 in Taillandier et al., 2006b). Here instead the current is present also in OSref.

Coming back to the LIW, the mean circulation at 350m (Figure 3) is similarly characterized for OSref and OStrj by an eastward flow, located offshore the Balearic Islands, in agreement with the path of the float. The trajectory assimilation tends to slightly slow down and to widen the current, as shown also by the pattern of the differences between OStrj and OSref in Figure 3c, and in agreement with what shown by the section in Figure 5 or by the surface circulation in Figure 3d. Moreover, the pathway of the LIW, marked in Figure 5 by the subsurface patch of salty waters (higher the 38.48 PSU), appear relocated closer to the coast thanks to trajectory assimilation. In effect, its core is located at 2.85°E in OSref (Figure 5a), at 2.90°E in OStrj (Figure 5b), which is more in agreement with a LIW vein flowing at the coast, as reported by Pinaut and Ganachaud (1999) and Schroeder et al. (2008).

d) Case of the Ligurian Sea

In the Ligurian Sea, the circulation system crossed by the section C (see Figure 1) is also composed of two boundary currents (Béthoux et al., 1982; Béthoux and Prieur, 1983; Sournia et al., 1990; Barth et al., 2005), the Northern Current flowing westward (Sammari et al., 1995) and the branch along the Corsican coast that flows inside the sea. the current flowing north along western Corsica appears to detach from the coast in OSref (Figure 3a), joining the loop of the Northern Current without entering the Ligurian Sea, on the contrary of what is shown by the ARGO trajectories. However this branch is also represented in the mean currents reconstructed from sea surface topography (Figure 3d), forming the cyclonic eddy obtained by Barth et al. (2005). Note that in the regional simulation of Barth et al. (2005), this structure is located inside the Ligurian Sea, trapped along the bathymetric contours (see Figure 1), so that the “branching” toward the Provençal basin is located downstream north of the Corsican coast.

The trajectory assimilation tends to relocate eastward this circulation pattern (Figure 3b), even though the high variability in the trajectory paths induces a quite complex feature in the correction (Figure 3c). The branch flowing inside the Ligurian Sea is intensified in OStrj, even though the cyclonic eddy that blocks the entrance along Corsica is not weakened. A possible explanation would be related to the imbalance of the two forcing responses that drive this regional circulation: a barotropic one governed by a permanent wind curl over the Ligurian Sea, and a baroclinic one governed by the doming reservoir of dense waters that spread eastward until the topographic break (Béthoux and Prieur, 1983, Béthoux et al., 1982). As the latter forcing is weakened because of an under-representation in the model climatology, the main driving force governed by the wind curl acts also in the deeper layers and stabilize this blocking cyclonic gyre represented in the two analyses (Prieur, personal communication).

As a consequence of this “branching” correction at the southwestern entrance of the Ligurian Sea, the circulation of the LIW is drastically influenced by the trajectory assimilation. As shown in Figure 6, the core of maximum salinity in subsurface, which characterizes the LIW, is well marked in the two analyses, situated along the western Corsican coast and directly sampled by two floats (Figure 1). Considering the vein delimited by the isohaline 38.52 PSU (in dark red color), this water mass appears located offshore between 600m and 800m deep in OSref (Figure 6a), and at the coast between 400m and 700m deep in OStrj (Figure 6b). The location of the LIW core obtained in OStrj appears in agreement with sections reported from historical field surveys (Sournia et al., 1990), that obtained a LIW core located at the coast and centered at 500m depth.

Moreover, the trajectory assimilation has an effect on the vertical structure of the velocity (Figure 6). The vein of LIW is located within the core of the boundary current flowing northwestward in OStrj, while in OSref is deeper than the boundary current and located at a more quiescent depth. The pattern depicted by OStrj appears more realistic, because according to historical measurements (Sournia et al., 1990) a persistent branch of LIW would follow the coastal pathway along the western coast of Corsica, without much penetrating the Provençal basin.

e) Case of the Algerian basin

We have seen in Section 4b the significant impacts due to trajectory assimilation in the Algerian basin, even if no ARGO float was drifting in this area during the period. The differences between the two analyses are now detailed in conjunction with historical Lagrangian observations realized in this basin (Testor and Gascard, 2005).

The misfits on the mean intermediate circulation (Figure 3) are generated by the assimilation of the ARGO trajectory drifting in the northern part of the Algerian basin, between the Balearic Islands and Corsica. During its motion from (39.8°N, 5.9°E) to (40°N, 6.3°E), this trajectory describes an anticyclonic shape whereas the underlying circulation appears mainly cyclonic in OSref (see Figure 3a). This large cyclonic structure may be considered as a model artefact, at least it has never been described by any subsurface float during the dedicated Lagrangian experiments (Testor and Gascard, 2005) nor by any ARGO float which has crossed this area. Moreover, there is no signature of such a structure in the reconstructed currents by sea surface topography (Figure 3d). As an alternative interpretation of this trajectory shape, the ARGO float may be trapped inside a so-called Sardinian eddy that has been generated along the western Sardinian shelf in the edge of the cyclonic Algerian gyre (Testor and Gascard, 2005; Testor et al., 2005a). This hypothesis is supported by the fact that Sardinian eddies do not show any signature on the surface layer, which is the case looking at the section B (Figure 4 at between 39°5N and 40.5°N).

As a result, the information of the anticyclonic shape strongly weakens the artefactual cyclonic gyre, which is shown in the mean circulation misfit (Figure 3c) by an energetic anticyclonic pattern extending between (39°N, 7°E) and (40.5°N, 5°E). This correction pattern will then influence the mesoscale eddy activity, which is quite significant in the Algerian basin (Taupier-Letage et al., 2003; Testor et al., 2005b). The most visible effect is the shift of the Algerian eddy centered at (38°N, 6°E) (Figure 3c), which has been already mentioned in Section 4b. As the northern component of the dipole is removed (Figure 3b), this eddy tends to be relocated westward in OStrj, which is in agreement with the surface signature given in Figure 3d. Such structure is in effect well depicted in the surface layer, as shown on the section B at 38.2°N. The increased deepening of the halocline in OStrj (Figure 4b) depicts the translation of the eddy core onto the section location, compared to OSref (Figure 4a) where the section B would sample the surrounding part of the structure.

A second remote effect of the correction pattern associated to trajectory assimilation is the intensification of the boundary current along the western Sardinian shelf. The artefactual cyclonic structure present in OSref would block the eastern branch of the Algerian gyre (at (39°N, 7°E) in Figure 3a). In OStrj, this blocking effect is removed and the large scale circulation can develop along the Sardinian shelf (between (38.5°N, 8°E) and (39°N, 7°E) in Figure 3b). Overall, the changes induced by the trajectory assimilation significantly affect the large scale LIW circulation in this basin by acting on its mesoscale features, which appear consistent with the well known patterns of the mean regional circulation. The fluctuations in time of the mean circulation are now to be addressed.

f) Impact on flow variability

Given the significant changes provided by trajectory assimilation on the mean flow (e.g. Figure 3c), one can expect also a consequent redistribution of eddy energy due to space and time shifts between and OStrj. At this point, two underlying investigations would be needed when assessing the trajectory integration. The first one is to map this redistribution and locate the energy inputs, the second one is to quantify the amplitude of the energy inputs and assess their consistency with respect to realistic levels. The third diagnostic described in Section 3c is considered in order to investigate these points.

The surface EKE differences, EKEdiff, are represented in Figure 7a. They can reach an amplitude up to 60 cm^2/s^2 in the Algerian basin where one can find the most intense changes in eddy energy distributions between the two analyses. The amplitudes are smaller in the northern part of the basin but one can notice several patches of magnitude ~10-20 cm^2/s^2. In the same figure, we can notice that the eddy energy is input (positive difference) in OStrj along three trajectories (the one in the Balearic Sea and the two in the Ligurian Sea), instead the eddy energy is removed (negative difference) along the trajectory between Balearic Islands and Sardinia. So energy inputs are mainly located on the boundary currents sampled by trajectories, while the energy is decreased in the open ocean structures such as the artefactual cyclonic gyre centered at (40°N, 6°E). These local energy changes influence the intensity of the neighboring structures, which is particularly well marked in the southern central area (tripolar shapes at (39°N, 6.5°E)) and more slightly at the entrance of the Balearic Sea (41°N, 4°E) or in the Ligurian Sea (43°N, 8°E).

The energy changes obtained along trajectories appear more clearly in the normalized EKE, EKEnorm, shown in Figure 7b. As it can be seen, relative differences exceed 50% of the reference value in regions directly sampled by the floats. On the other hand, changes in the neighborhood are relatively quiescent, specially in the southern central area characterized by high eddy energy levels. So the energy inputs generated by the trajectory assimilation appear relatively consistent in amplitude as the most intense patches given by EKEdiff correspond to relatively weak changes with respect to the reference eddy energy distributions.

Overall, changes due to trajectory assimilation can be quite intense in energetic areas of the flow, but they are relatively significant mostly at the locations sampled by trajectories. More precisely, eddy energy is input by trajectory assimilation in the sampled coastal areas where turbulent energy levels were low: this marks a more accurate representation of the variability of boundary currents. On the energetic areas, the mesoscale activity appears reorganized by the trajectory assimilation. In our particular case, trajectory information tends to locally reduce the eddy energy levels, that in consequence remotely influence the position and shape of intense mesoscale eddies such as the one in the Algerian basin (Section 4e).

g) Transports through the Corsica Channel

The transport computed in the Corsica Channel (through the section D, see Figure 1) from OSref and OStrj is compared with in-situ measurements in Figure 8. We recall that one ARGO trajectory is present in the neighborhood of this section (see Figure 1), even though it does not directly crosses the Corsica Channel. The influence of trajectory assimilation at the strait location is clearly marked in the mean circulation (Figure 3c) as well as in its variability (patches around (43°N, 8°E) in Figure 7).

The observation time series (black line in Figure 8) show the occurrence of significant fluctuations during the considered period, reaching minimum values of 0.7Sv and maximum values of 1.6Sv. The associated standard deviation to the 4-day average values (gray envelope) also fluctuate significantly up 0.3Sv. The mean value over the period (straight black line) is of 1.12Sv directed northward through the strait. The OSref time series (blue line) appear to follow quite closely the observation oscillations and stay inside the gray envelope at least up to the beginning of March. Its phase appears also quite consistent with observations up to February 20th. After the beginning of March, a slight phase shift (~3-7 days) can be observed, with the OSref results tending to lag behind the observations, and analyzed transports leave the observation envelope. After mid-March, a more significant departure from observation is observed, with the observations showing a strong decrease in the northward transport that is not present in OSref. This is reflected also on the mean transport value that is higher for OSref, 1.19Sv (straight blue line).

The results for OStrj (red line) maintain close to OSref up to the beginning of March, when the presence of a nearby trajectory starts to influence more strongly the transport. At this point, the transport appears significantly corrected and shows a decrease around March 10-15 that is not present in OSref. The correction is more in keeping with the observations, even though the difference with the observations is still significant. The mean transport over the period is lower than for OSref and it coincides exactly with the one of the observations, 1.11Sv (red straight line). This effect is shown also by the differences in the mean circulation (Figure 6c), indicating a southward difference flow in the Channel. Overall, the assimilation of the trajectories, while maintaining the basic transport features, appears to improve the results of OSref especially when a trajectory is nearby. Such insight appears particularly promising for the increased interest and important contribution of assimilating trajectories in near coastal areas and straits.

As an interesting side note, we qualitatively compare the results in Figure 8 with the analogous results obtained in Taillandier et al (2006b) (Figure 5 of the article) considering as reference a free run (i.e. with no assimilation) and adding the assimilation of trajectories in isolation. Overall, the results in Taillandier et al (2006b) appear significantly less energetic, therefore indicating that the assimilation of the MFS observing system significantly improves the realism of the energy level. Also, the free run in Taillandier et al. (2006b) was underestimating the mean northward transport, and the trajectory assimilation contributed to intensify it. In the present case, the inverse is observed, with a reference overestimating the mean northward transport, and the trajectory assimilation acting as to reduce the transport. This contributes to show the consistency of the transport correction in presence of trajectory assimilation. Finally, we observe that the shift noticed in Figure 8 between the observed fluctuations and the analyzed ones is also present and reinforced in Taillandier et al (2006b). This suggests that the shift could be due to an inherent delay in the model answer to atmospheric forcing, mainly due to the forcing time resolution. More investigations will be needed to assess this point.

5. Summary and concluding remarks

This study reports the first results obtained assimilating simultaneously ARGO trajectories together with their profile data and satellite altimeters SLA. It has been lead using the Mediterranean Forecasting System in which ARGO float position data have been integrated in its observing system. Short term analyses have been performed to identify the contribution and the consistency of such Lagrangian subsurface observations among the reference data distribution, and also to identify the circulation features that are better represented when assimilating ARGO trajectories in addition to satellite altimeters and profilers data.

Regarding the self consistency of the new forecasting system, the results show that the trajectory assimilation does not deteriorate the analysis of the ARGO profiles, but it contributes to refine the model error structure. More precisely, the isotropic correction provided by TS profiles is augmented by a correction of the TS horizontal gradient (hence of the hydrostatic pressure gradient) at the same location and time, in a direction orthogonal to the drift of the floats. As a consequence, the analysis benefits of a more accurate description of the boundary currents sampled by ARGO trajectories, because the model error structure accounts for the anisotropic pattern of hydrostatic pressure gradients (mainly in the cross-shore direction). Note that this information is not either well resolved by the other components of the observing system for a regional environment such as the Mediterranean Sea.

Regarding the impacts of trajectory assimilation, the sensitivity study lead on the seasonal mean circulation and its variability showed that changes were quite intense in energetic areas, relatively significant at locations sampled by trajectories (local influence), and more surprisingly far away from them (as remote influence). Correction patterns are depicted as spatial and temporal shifts of circulation features, acting on the relocation of eddies (shown in the Provençal and Algerian basins) or on the meanders associated to boundary currents (shown in the Balearic Sea and Ligurian Sea). These correction patterns generate a basin scale reorganization of the mesoscale eddy activity. In coastal areas where turbulent energy levels were low, eddy energy inputs appear relatively significant (in the Balearic Sea). On the other hand in energetic areas, local reductions of eddy energy levels remotely influence the position and shape of mesoscale structures (case of the Algerian eddy).

The impact of the trajectory assimilation is particularly sensitive on the Mediterranean Sea which basin scale circulation is mainly composed and driven by mesoscale structures. That is why the correction patterns obtained in this sensitivity study have been detailed and assessed with respect to historical and contemporary datasets. At the regional level, we saw that the width and the intensity of boundary currents sampled by trajectories were qualitatively improved (along the Balearic Islands) as well as the location of their branching toward the interior basin (at the entrance of the Ligurian Sea). The distribution of the water masses was also qualitatively improved, especially for the LIW which pathway at the coast and at appropriate depth appears in better agreement with historical datasets. At the basin scale level, the local modification of mesocale features leads to significant impacts on the large scale circulation, by for example acting on blocking structures (in the western Sardinian shelf, in the Ligurian Sea). A quantitative assessment considering the net transport at the Corsica Channel has shown the improvement of this mesoscale influence on the large scale circulation (Section 4g).

The results obtained by this short-term analysis motivate to perform a reanalysis of the whole Mediterranean circulation taking into account float trajectories stating from 1997 when profilers started to to be deployed (Testor et al., 2005b). As the main features of the circulation are driven by boundary currents, a more accurate characterization of their dynamics obtained using ARGO trajectories can allow to refine the energetic balances associated to the thermohaline circulation. Note also that a particular effort needs to be done for the representation of the Northern Current and the undercurrent LIW circulation over the Provençal basin, by acting on the climatological initialization to settle a consistent deep water reservoir, and by acting on the observing system using dedicated autonomous platforms such gliders (Niewiadomska et al., 2008) or instrumented moorings.

The present methodology and associated skills open perspective avenues toward the integration of trajectory data in forecasting systems operating in other regions, given that ARGO floats are an integral and fundamental part of the word oceans observing system (reaching nowadays 3000 profilers deployed). So, the full exploitation of their information is expected to be of great benefit for prediction. Longer term perspectives are also opened considering other in-situ automated quasi-Lagrangian platforms such as surface drifters and gliders that would also provide fruitful information for an improved representation of mesoscales in future re-analyses and forecasts.

Acknowledgments

We would like to acknowledge Karine Béranger and Louis Prieur for fruitful discussions, as well as Pierre-Marie Poulain and the MedARGO team that deployed the profilers and processed the data. The altimeter products were provided by Ssalto/Duacs and distributed by Aviso with the kind support of Stéphanie Guinehut from CLS. VT was funded by the French ANR under the grant LIVINGSTONE.

References

Astraldi, M., M. Balopoulos, J. Candela, J. Font, M. Gacic, G.-P. Gasparini, B. Manca, A. Theocharis, and J. Tintore (1999). The role of straits and channels in understanding the characteristics of Mediterranean circulation. *Progress in Oceanography*, 44, 65-108.

Barth, A., A. Alvera-Azcarate, M. Rixen, and J.M. Beckers (2005). Two-way nested model of mesoscale circulation features in the Ligurian Sea. *Journal of Marine Systems*, 66, 171-189.

Béranger, K., L. Mortier, and M. Crépon (2005). Seasonal variability of water transport through the straits of Gibraltar, Sicily and Corsica, derived from a high-resolution model of the Mediterranean circulation. *Progress in Oceanography,* 2-4, 341-364.

Béthoux, J.P., L. Prieur, and F. Nyffeler (1982). The water circulation in the north-western Mediterranean Sea, its relations with wind and atmospheric pressure. in: Nihoul, J.C.J. (Ed.). Hydrodynamics of semi-enclosed seas: Proceedings of the 13th International Liège Colloquium on Ocean Hydrodynamics. *Elsevier Oceanography Series*, 34, 129-142.

Béthoux, J.P., and L. Prieur (1983). Hydrologie et circulation en Méditerranée nord-occidentale. *Pétrole Technique*, 299, 25-34.

Bouzinac, C., J. Font and C. Millot (1999). Hydrology and currents observed in the channel of Sardinia during the PRIMO-1 experiment from November 1993 to October 1994. *Journal of Marine Systems*, 20, 333-355.

Buongiorno Nardelli, B., G. Larnicol, E. D'Acunzo, R. Santoleri, S. Marullo, and P.Y. Le Traon (2003). Near real time SLA and SST products during 2 years of MFS pilot project : processing, analysis of the variability and of the coupled patterns. *Annales Geophysicae*, 21, 103-121.

Crépon M., L. Wald, and J.M. Longuet (1982). Low frequency waves in the Ligurian Sea during December 1977. *Journal of Geophysical Research*, 87, 595-600.

Demirov, E., and N. Pinardi (2007). On the relationship between the water mass pathways and eddy variability in the Western Mediterranean Sea. *Journal of Geophysical Research*, 112, C02024.

Deschamps, P.Y., R. Frouin, and M. Crépon (1984). Sea surface temperatures of the coastal zones of France observed by the HCMM satellite. *Journal of Geophysical Research*, 89, 81238149.

Dobricic, S., N. Pinardi, M. Adani, A. Bonazzi, C. Fratianni, and M. Tonani (2005). Mediterranean Forecasting System: An improved assimilation scheme for sea-level anomaly and its validation. *Quarterly Journal of the Royal Meteorological Society*, 131, 3627-3642.

Dobricic, S., N. Pinardi, M. Adani, M. Tonani, C. Fratianni, A. Bonazzi, and V. Fernandez (2007). Daily oceanographic analyses by the Mediterranean basin scale assimilation system. *Ocean Science*, 3, 149-157.

Dobricic, S., N. Pinardi, P. Testor, and U. Send. Data assimilation of glider observations in the Ionian Sea (Eastern Mediterranean): a study of the path of the Atlantic Ionian Stream. *Journal of Physical Oceanography*, in revision.

Dobricic, S., and N. Pinardi (2008). An oceanographic three-dimensional variational data assimilation scheme. *Ocean Modelling*, 22, 3-4, 89-105.

Font, J., J. Salat, and J. Tintoré (1988). Permanent features of the circulation in the Catalan Sea. *Oceanologica Acta*, 9, 51-57.

Ide, K., L. Kuznetsov, and C.K.R.T. Jones (2002). Lagrangian data assimilation for point vortex systems. *Journal of Turbulence*, 3, 53-59.

Ishikawa, Y.I., T. Awaji, and K. Akimoto (1996). Successive correction of mean sea surface height by the simulatneous assimilation of drifting buoys and altimetric data. *Journal of Physical Oceanography*, 26, 2381-2397.

Kamachi, M., and J.J. O'Brien (1995). Continuous assimilation of drifting buoy trajectories into an equatorial Pacific Ocean model. *Journal of Marine Systems*, 6, 159–178.

Kuznetsov, L., K. Ide, and C.K.R.T. Jones (2003). A method for assimilation of lagrangian data. *Monthly Weather Review*, 131, 2247–2260.

LaViolette, P. E., J. Tintoré, and J. Font (1990). The surface circulation of the Balearic Sea, *Journal of Geophysical Research*, 95, 1559–1568.

Le Traon, P.Y., F. Nadal, and N. Ducet (2003). An improved mapping method of multisatellite altimeter data. *Journal of Atmospheric and Oceanic Technology*, 15, 522-533.

Madec, C., F. Lott, P. Delecluse, and M. Crépon (1996). Large scale preconditioning of deep water formation in the north-western Mediterranean sea. *Journal of Physical Oceanography*, 26, 1393-1408.

Manzella, G.M.R., F. Reseghetti, G. Coppini, M. Borghini, A. Cruzado, C. Galli, I. Gertman, T. Gervais, D. Hayes, C. Millot, A. Murashkovsky, E. Özsoy, C. Tziavos, Z. Velasquez, and G. Zodiatis (2007). The improvements of the ships of opportunity program in MFSTEP. *Ocean Science*, 3, 245-258.

Mariano, A.J., T.M. Chin, and T.M. Ozgokmen (2003). Stochastic boundary conditions for modeling of coastal flows. *Geophysical Research Letters*, 30, GL016972.

Marullo, S., B. Buongiorno Nardelli, M. Guarracino, and R. Santoleri (2007). Observing the Mediterranean Sea from space: 21 years of pathfinder-AVHRR sea surface temperatures (1985-2005): re-analysis and validation. *Ocean Science*, 3, 299-310.

Millot, C. (1985). Some features of the Algerian current. *Journal of Geophysical Research*, 90, 7169-7176.

Millot, C. (1999). Circulation in the Western Mediterranean Sea. *Journal of Marine Systems*, 20, 423-442.

Molcard, A., A. Griffa, and T.M. Ozgokmen (2005). Lagrangian data assimilation in multi-layer primitive equation ocean models. Journal of Atmospheric and Oceanic Technology, 22, 70–83.

Molcard, A., L.I. Piterbarg, A. Griffa, T.M. Ozgokmen, and A.J. Mariano (2003). Assimilation of drifter positions for the reconstruction of the eulerian circulation field. *Journal of Geophysical Research*, 108, 3056.

Niewiadomska, K., H. Claustre, L. Prieur, and F. d'Ortenzio (2008). Submesoscale physical-biogeochemical coupling across the Ligurian current (northwestern Mediterranean) using a bio-optical glider. *Limnology and Oceanography*, 53, 2210-2225.

Nittis, K., C. Tziavos, R. Bozzano, V. Cardin, Y. Thanos, G. Petihakis, M.E. Schiano, and F. Zanon (2007). The M3A multi-sensor buoy network of the Mediterranean Sea. *Ocean Science*, 3, 229-243.

Nodet, M. (2006). Variational assimilation of Lagrangian data in oceanography. *Inverse Problems*, 22, 245-263.

Ozgokmen, T.M., A. Griffa, L.I. Piterbarg, and A.J. Mariano (2000). On the predictability of the Lagrangian trajectories in the ocean. *Journal of Atmospheric and Oceanic Technology*, 17, 366–383.

Pascual, A., B. Buongiorno Nardelli, G. Larnicol, M. Emelianov, and D. Gomis (2002). A case of an intense anticyclonic eddy in the Balearic Sea (western Mediterranean). *Journal of Geophysical Research*, 107, 3183.

Pinardi, N., I. Allen, E. Demirov, P. De Mey, G. Korres, A. Lascaratos, P.-Y. Le Traon, C.Maillard, G. Manzella, and C. Tziavos (2003). The Mediterranean ocean forecasting system: first phase of implementation (1998-2001). *Annales Geophysicae*, 21, 3-20.

Pinot, J.M., J.L. Lopez-Jurado and M. Riera (2002). The CANALES experiment (1996-1998). Interannual, seasonal, and mesoscale variability of the circulation in the Balearic Channels. *Progress in Oceanography*, 55, 335-370.

Pinot, J.-M., and A. Ganachaud (1999). The role of winter intermediate wters in the spring-summer circulation of the Balrearic Sea. 1. Hydrography and inverse box modeling. *Journal of Geophysical Research*, 104, 29843-29864.

Poulain, P.M., R. Barbanti, J. Font, A. Cruzado, C. Millot, I. Gertman, A. Griffa, A. Molcard, V. Rupolo, S. Le Bras, and L. Petit de la Villeon (2007). MedARGO: a drifting profiler program in the Mediterranean Sea. *Ocean Science*, 3, 379-395.

Puillat, I., I. Taupier-Letage, and C. Millot (2002). Algerian eddies can span near three years. *Journal of Marine Systems*, 31, 245-259.

Rio, M.-H., P.-M. Poulain, A. Pascual, E. Mauri, G. Larnicol, and R. Santoleri (2007). A Mean Dynamic Topography of the Mediterranean Sea computed from altimetric data, in-situ measurements and a general circulation model. *Journal of Marine Systems*, 65, 484-508.

Sammari, C., C. Millot, and L. Prieur (1995). Aspects of the seasonal and mesoscale variabilities of the Northern Current in the western Mediterranean Sea inferred from the PROLIG-2 and PROS-6 experiments. *Deep-Sea Research Part 1*, 42, 893-917.

Schroeder K., V. Taillandier, A. Vetrano, and G.-P. Gasparini (2008). The circulation of the Western Mediterranean Sea in spring 2005 as inferred from observations and from model outputs. *Deep-Sea Research Part 1*, 55, 947-965.

Sournia, A., J.M. Brylinski, S. Dallot, P. Le Corre, M. Leveau, L. Prieur, and C. Froget (1990). Fronts hydrologiques au large des côtes françaises: les sites-ateliers du programme Frontal. *Oceanologica Acta*, 13, 413-438.

Ssalto/Duacs User handbook (2006). (M)SLA and (M)ADT near-real time and delayed time products. *CLS-DOS-NT-06.034*.

Taillandier, V., A. Griffa, P.M. Poulain, R. Signell, J. Chiggiato and S. Carniel (2008). Variational analysis of drifter positions and model outputs for the reconstruction of surface currents in the Central Adriatic during fall 2002. *Journal of Geophysical Research*, 113, JC004148.

Taillandier, V., A. Griffa, and A. Molcard (2006a). A variational approach for the reconstruction of regional scale Eulerian velocity fields from Lagrangian data. *Ocean Modelling*, 13, 1-24.

Taillandier, V., A. Griffa, P.-M. Poulain, and K. Béranger (2006b). Assimilation of ARGO float positions in the North Western Mediterranean Sea and impact on ocean circulation simulations. *Geophysical Research Letters*, L11604.

Taillandier, V., and A. Griffa (2006). Implementation of a position assimilation method for ARGO floats in a Mediterranean Sea OPA model and twin experiment testing. *Ocean Science*, 2, 223-236.

Taupier-Letage, I., I. Puillat, P. Raimbault, and C. Millot (2003), Biological response to mesoscale eddies in the Algerian Basin. *Journal of Geophysical Research*, 108, 3245-3267.

Testor, P., K. Béranger, and L. Mortier (2005a). Modeling the deep eddy field in the south-western Mediterranean: the life cycle of Sardinian eddies. *Geophysical Research Letters*, 32, L13602.

Testor, P., U. Send, J.C. Gascard, C. Millot, I. Taupier-Letage, and K. Béranger (2005b). The mean circulation of the southwestern Mediterranean Sea - the Algerian Gyres. J*ournal of Geophysical Research*, 110, C11017.

Testor, P., and J.-C. Gascard (2006). Post convection spreading phase in the north-western Mediterranean Sea. *Deep Sea Research Part I*, 53, 869-893.

Testor, P., and J.-C. Gascard (2005). Large scale flow separation and mesoscale eddy formation in the Algerian Basin. *Progress in Oceanography*, 66, 211-230.

Tonani, M., N. Pinardi, S. Dobricic, I. Pujol and C. Fratianni (2008). A high resolution free surface model of the Mediterranean Sea. *Ocean Science*, 4, 1-14.

Figure caption list

Figure 1: Trajectories of four ARGO floats inside the NW Mediterranean. The four sections of the Balearic Sea (A), the Algero-Provençal basin (B), the Ligurian Sea (C), and Corsica Channel (D) are also indicated in straight line superimposed on the isobaths 500m, 1000m, 2000m.

Figure 2: The root mean square of temperature misfits (^{o}C, left panel) and salinity misfits (PSU, right panel) in the period January-March 2005 for the four ARGO profilers. The full line represents the result in OSref (without trajectory assimilation), and the dashed line in OStrj (with trajectory assimilation).

Figure 3: a) Mean circulation at 350m computed from OSref. b) Mean circulation at 350m computed from OStrj. c) Difference between the two flows at 350m (OStrj minus OSref). d) Mean circulation computed from Currents reconstructed by sea surface topography (Aviso product). The velocities (in cm/s) are superimposed on the amplitude (in cm/s) of the currents, as well as the four ARGO trajectories and the four sections.

Figure 4: Mean stratification along the section B (Algero-Provençal basin). a) Salinity (in PSU) extracted daily from the analysis OSref, and averaged during the period January 1 – March 31, 2005. b) Same as a) for the analysis OStrj. Contours: absolute velocities normal to the section (in cm/s, every 5cm/s) averaged over the same period.

Figure 5: same as Figure 3 along the section A (Balearic Sea).

Figure 6: same as Figure 3 along the section C (Ligurian Sea). Contours: absolute velocities normal to the section (in cm/s, every 1cm/s) averaged over the same period.

Figure 7: Comparison of the mean EKE as obtained by the two analyzed surface flows over the period January 1 – March 31, 2005. a) EKEdiff, computed as difference between OStrj and OSref (in cm^2/s^2). b) EKEnorm, computed as absolute EKE difference normalized by the EKE of reference. The two maps have been regridded at a 1/8 degree resolution and low-pass filtered with a cut-off radius of 10km. The four ARGO trajectories are also superimposed.

Figure 8: Evolution of the net transport crossing the section of the Corsica Channel. Plot in blue corresponds to OSref, in red to OStrj, and in black to the independent observation by moored current meter. The envelope of admissible values with respect to the standard deviation of the observed transports is indicated in grey. The mean transports over the period are also plotted by the straight lines. The time-series from the two analyses have been low-pass filtered with a cut-off period of 4 days.

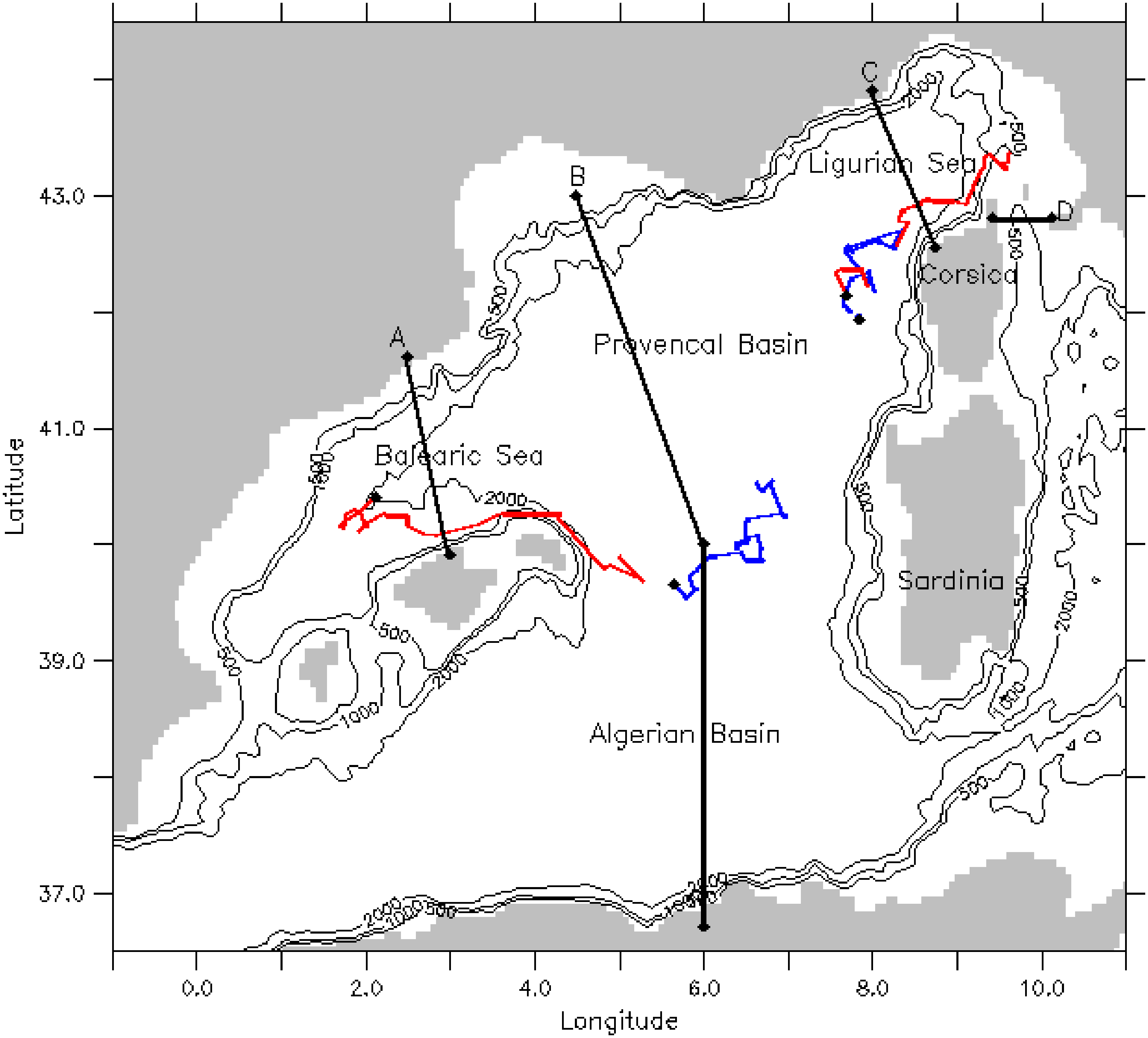
C
B
A
D
Ligurian Sea
Corsica
Provencal Basin
Balearic Sea
Sardinia
Algerian Basin
500
1000
2000
43.0
41.0
39.0
37.0
0.0
2.0
4.0
6.0
8.0
10.0
Latitude
Longitude

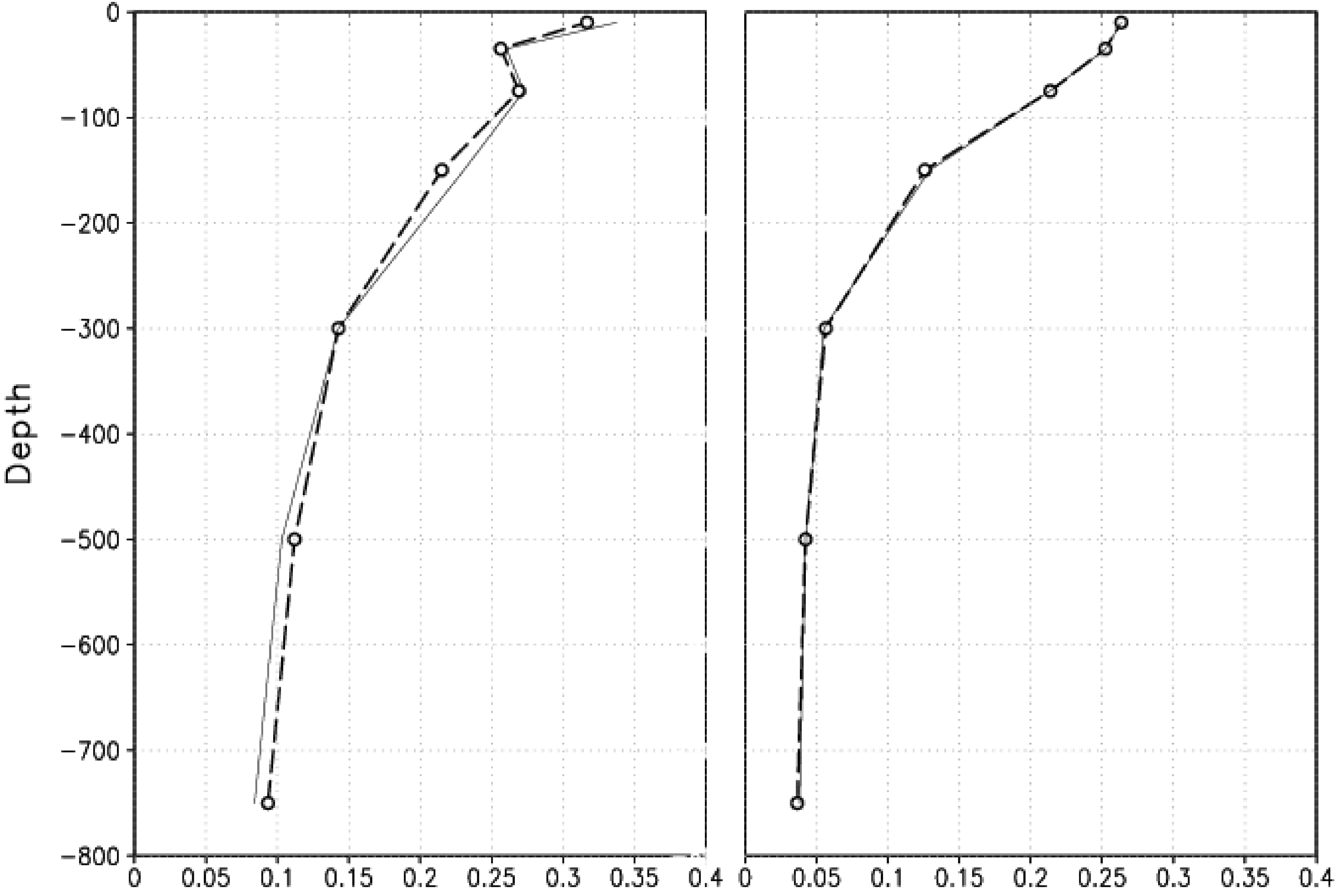
Depth
0
−100
−200
−300
−400
−500
−600
−700
−800
0
0.05
0.1
0.15
0.2
0.25
0.3
0.35
0.4
0
0.05
0.1
0.15
0.2
0.25
0.3
0.35
0.4

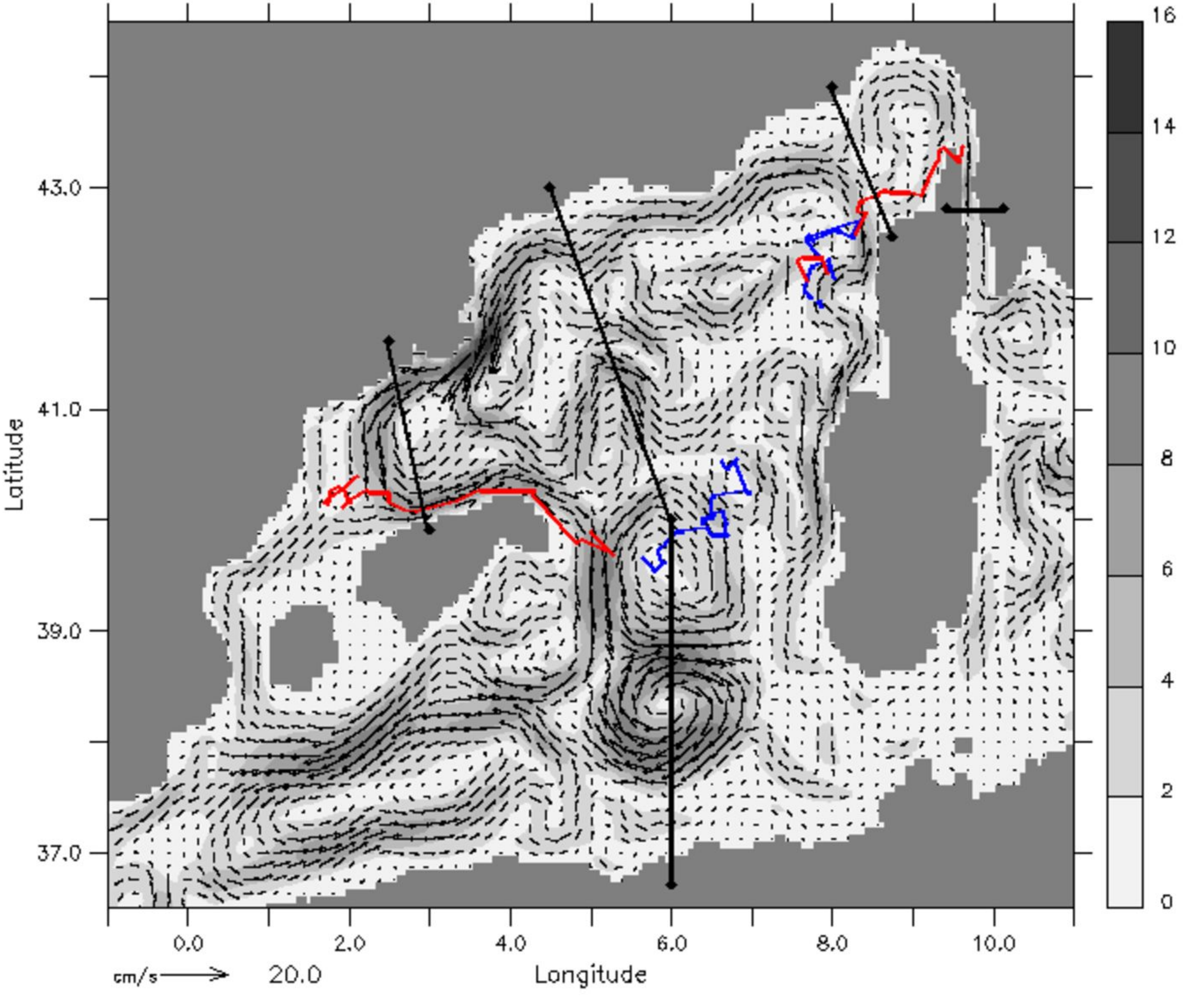
16
14
12
10
8
6
4
2
0
43.0
41.0
39.0
37.0
Latitude
0.0
2.0
4.0
6.0
8.0
10.0
Longitude
cm/s
20.0

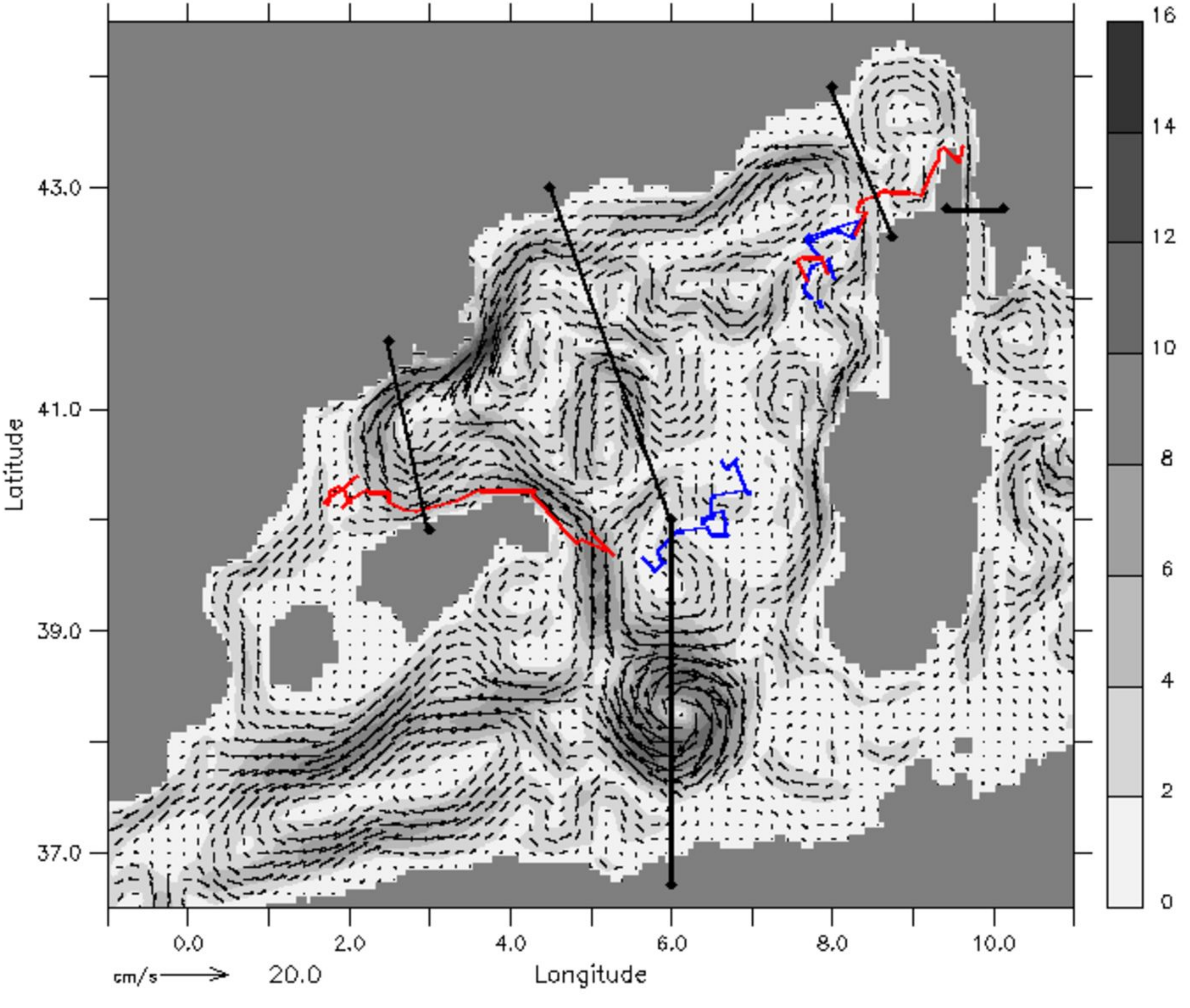

43.0
41.0
39.0
37.0
Latitude
0.0
2.0
4.0
6.0
8.0
10.0
Longitude
cm/s
20.0
16
14
12
10
8
6
4
2
0

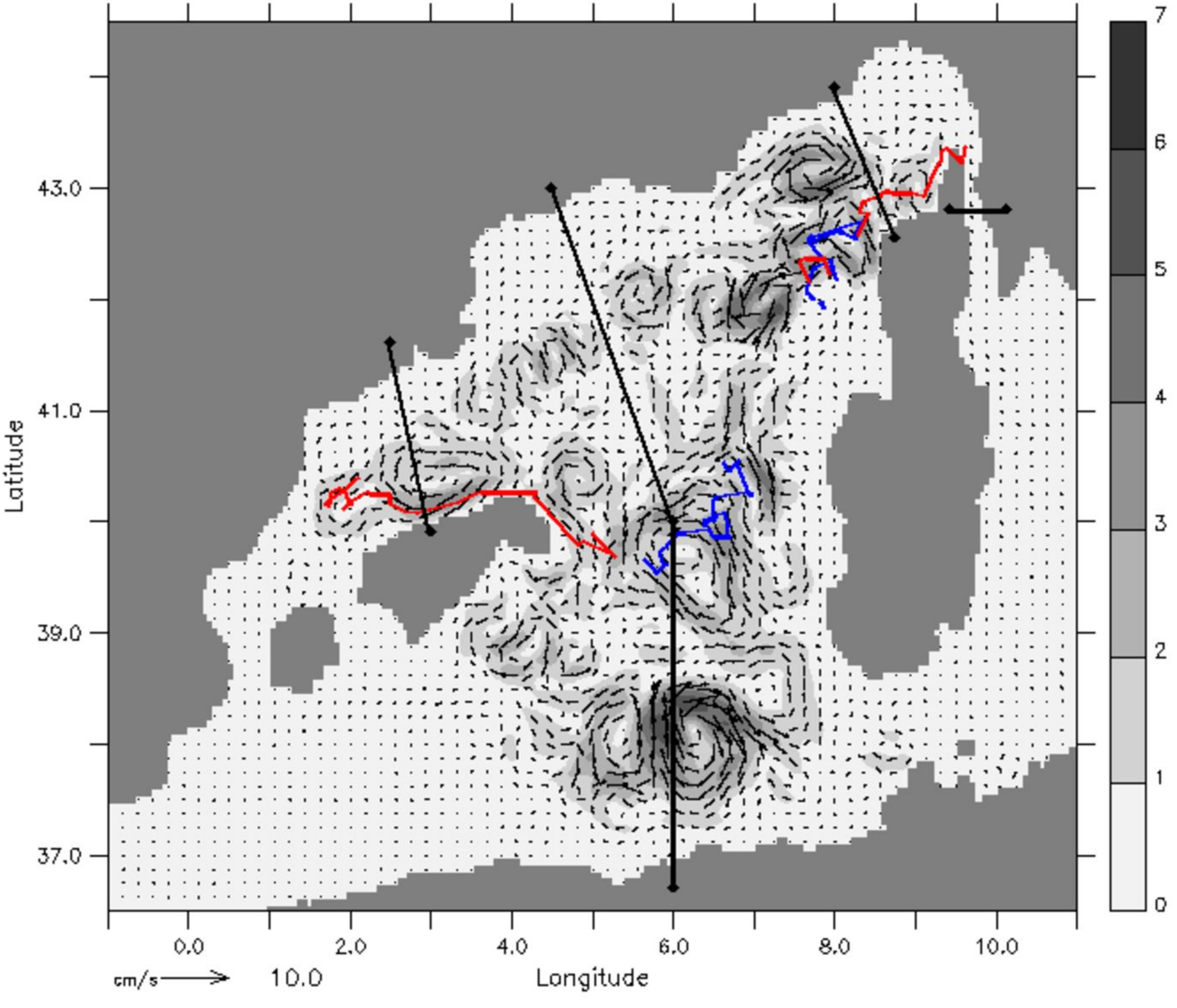
43.0
41.0
39.0
37.0
Latitude
0.0
2.0
4.0
6.0
8.0
10.0
Longitude
cm/s
10.0
7
6
5
4
3
2
1
0

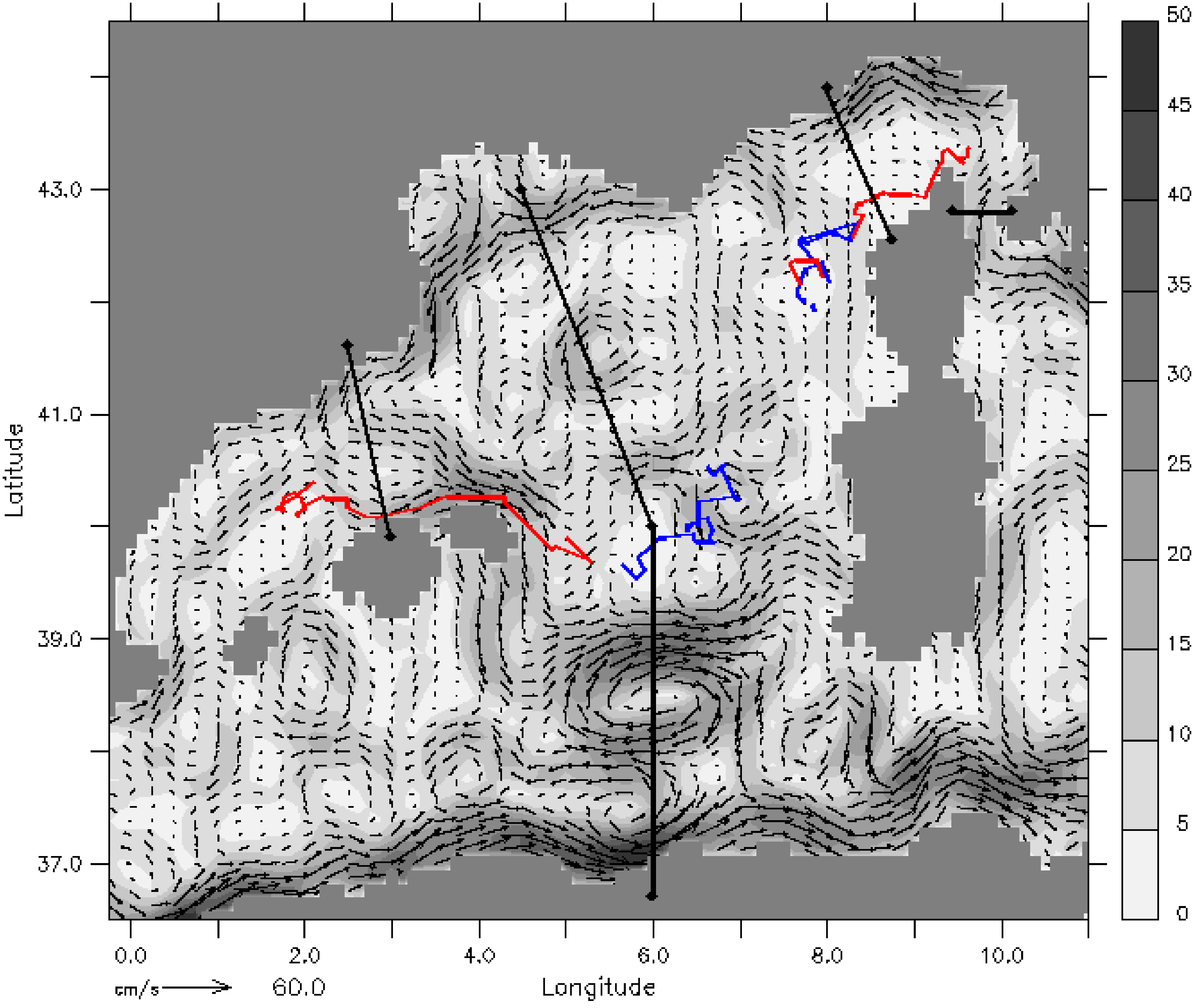
50
45
40
35
30
25
20
15
10
5
0
43.0
41.0
39.0
37.0
Latitude
0.0
2.0
4.0
6.0
8.0
10.0
Longitude
cm/s
60.0

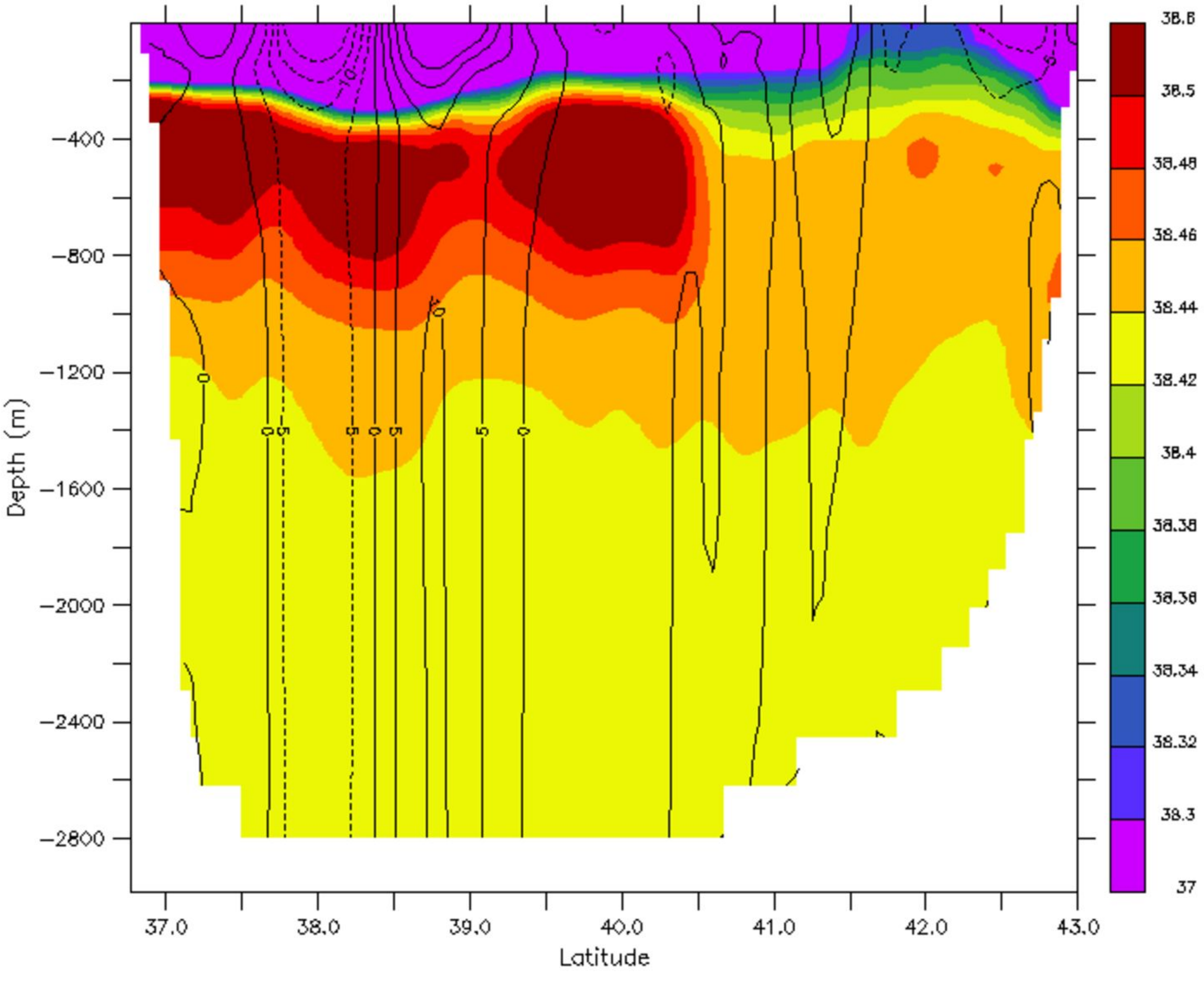
Depth (m)
-400
-800
-1200
-1600
-2000
-2400
-2800
Latitude
37.0
38.0
39.0
40.0
41.0
42.0
43.0
38.6
38.5
38.48
38.46
38.44
38.42
38.4
38.38
38.36
38.34
38.32
38.3
37
-10
0
5

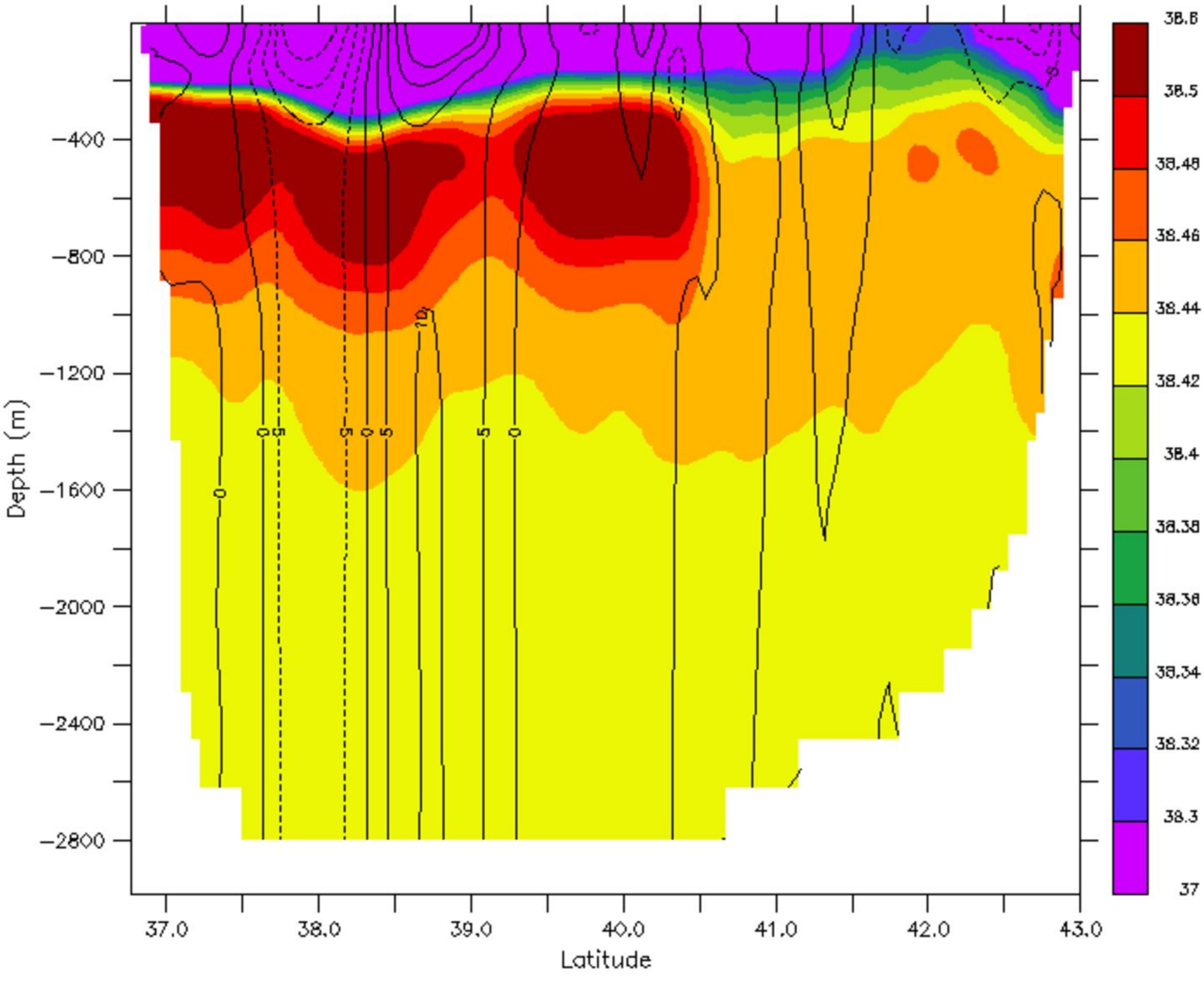
Depth (m)
-400
-800
-1200
-1600
-2000
-2400
-2800
Latitude
37.0
38.0
39.0
40.0
41.0
42.0
43.0
38.6
38.5
38.48
38.46
38.44
38.42
38.4
38.38
38.36
38.34
38.32
38.3
37
0
5
10

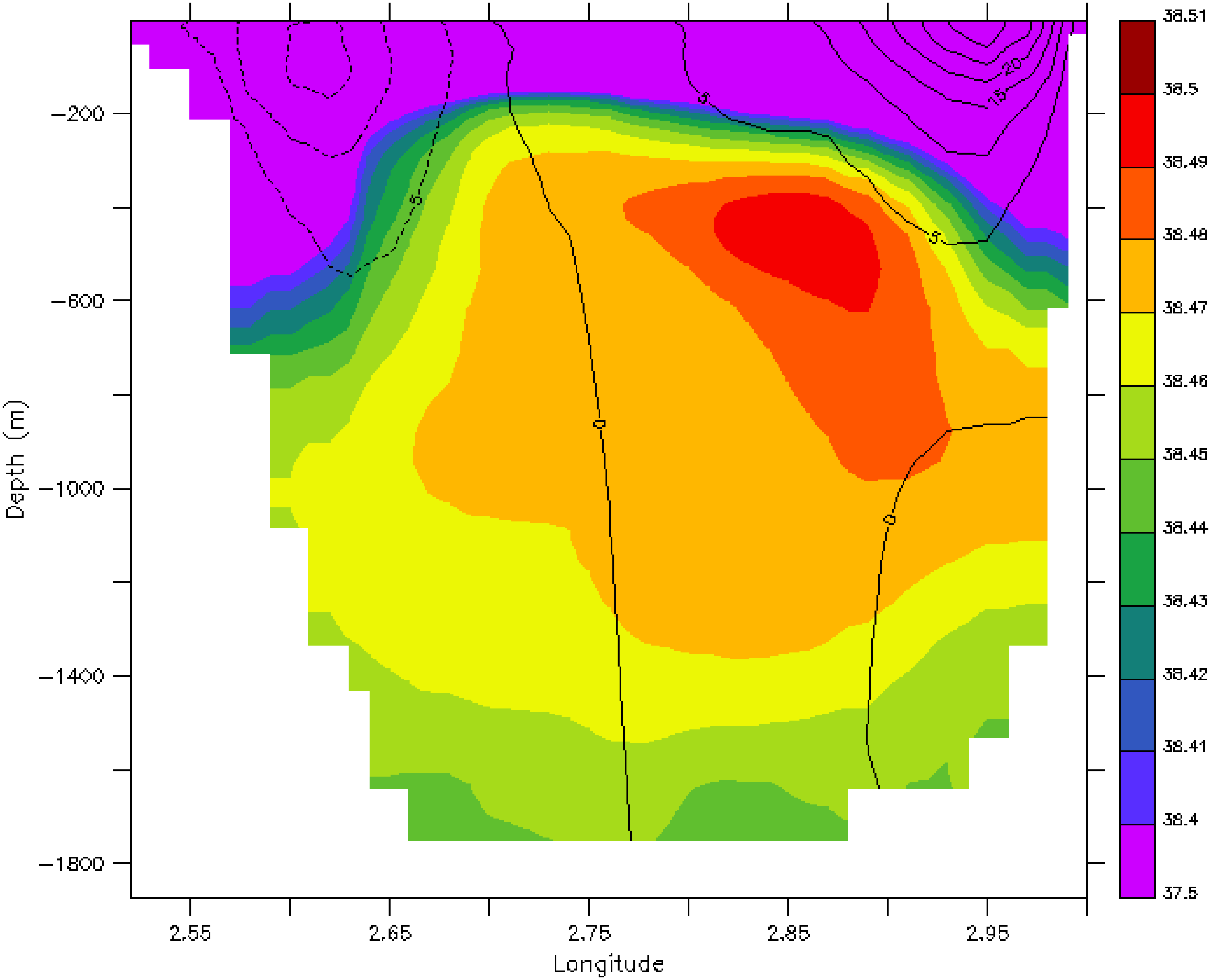
Depth (m)
-200
-600
-1000
-1400
-1800
Longitude
2.55
2.65
2.75
2.85
2.95
5
0
15
20
38.51
38.5
38.49
38.48
38.47
38.46
38.45
38.44
38.43
38.42
38.41
38.4
37.5

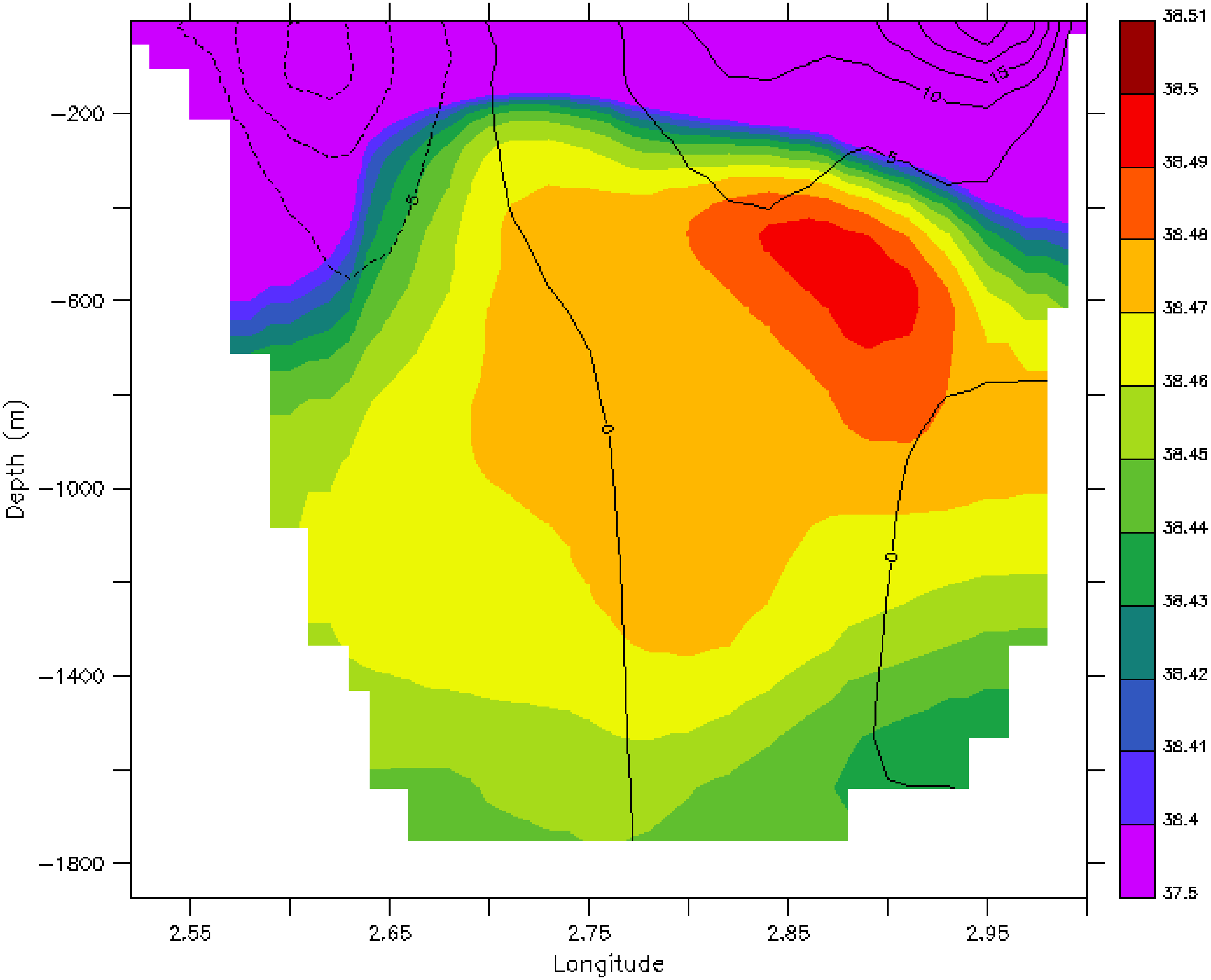

−200
−600
−1000
−1400
−1800
Depth (m)
2.55
2.65
2.75
2.85
2.95
Longitude
15
10
5
5
0
0
38.51
38.5
38.49
38.48
38.47
38.46
38.45
38.44
38.43
38.42
38.41
38.4
37.5

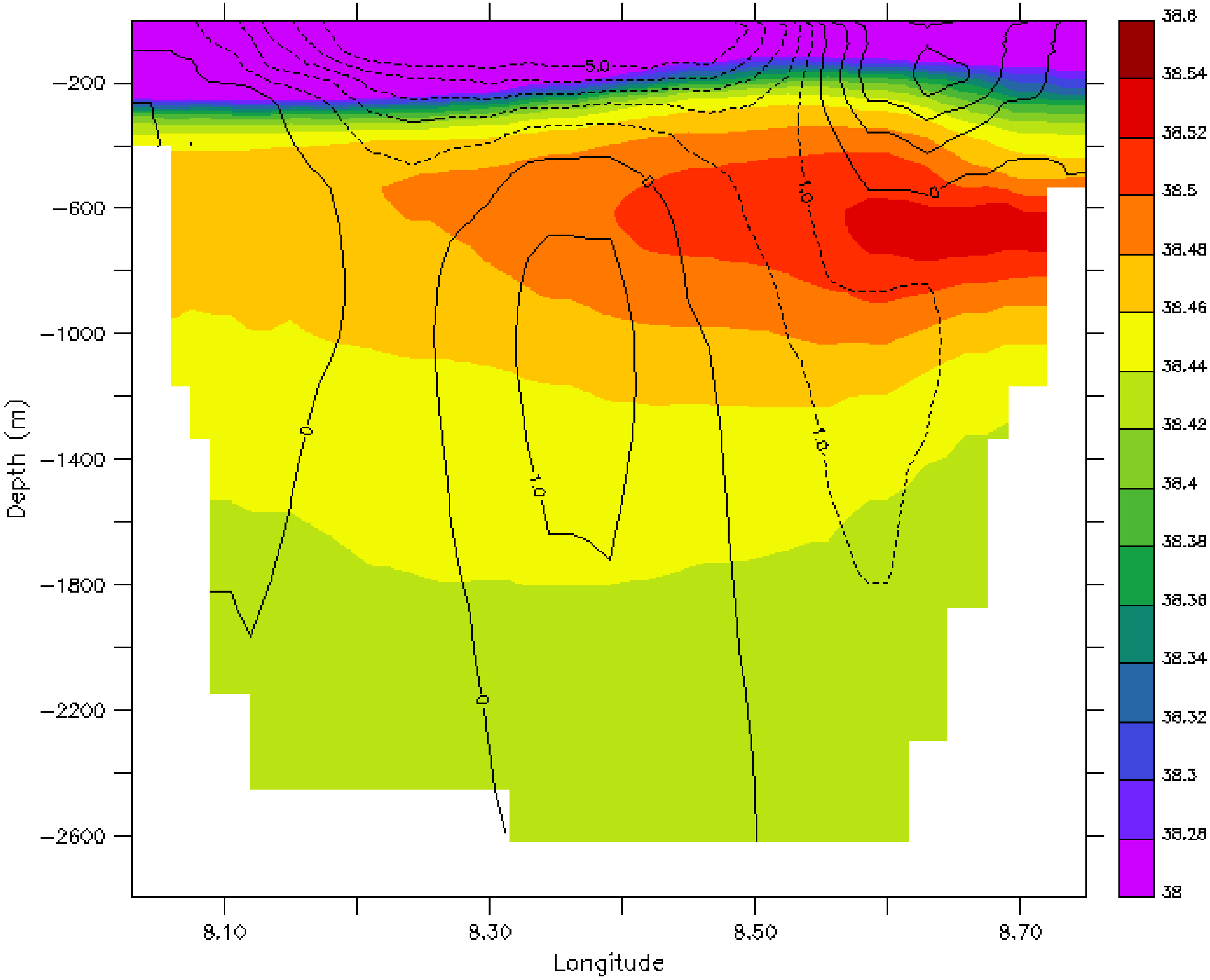
-200
-600
-1000
-1400
-1800
-2200
-2600
Depth (m)
8.10
8.30
8.50
8.70
Longitude
5.0
0
0
1.0
1.0
1.0
0
0
0
38.6
38.54
38.52
38.5
38.48
38.46
38.44
38.42
38.4
38.38
38.36
38.34
38.32
38.3
38.28
38

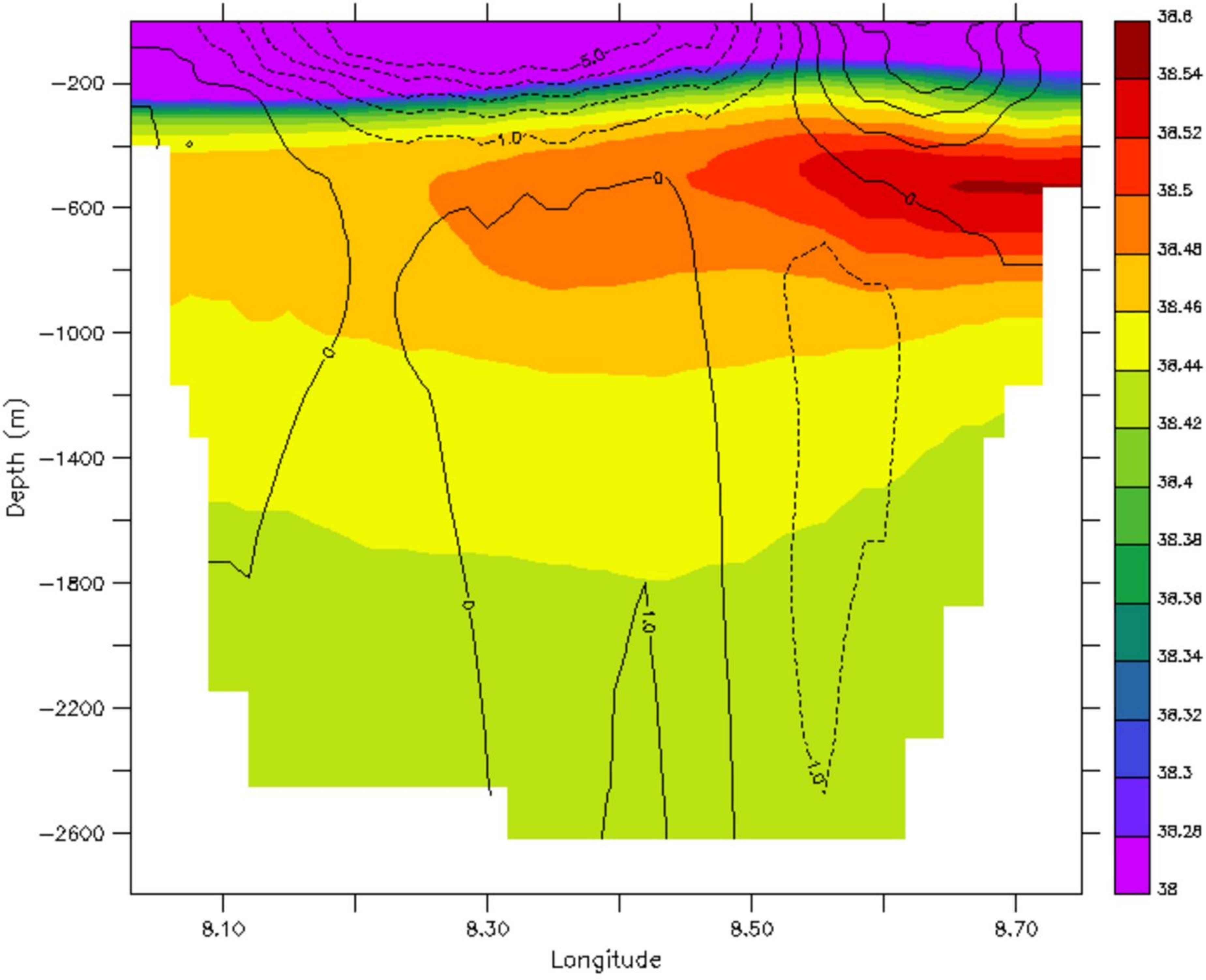
-200
-600
-1000
-1400
-1800
-2200
-2600
Depth (m)
8.10
8.30
8.50
8.70
Longitude
-5.0
-1.0
0
1.0
-1.0
38.6
38.54
38.52
38.5
38.48
38.46
38.44
38.42
38.4
38.38
38.36
38.34
38.32
38.3
38.28
38

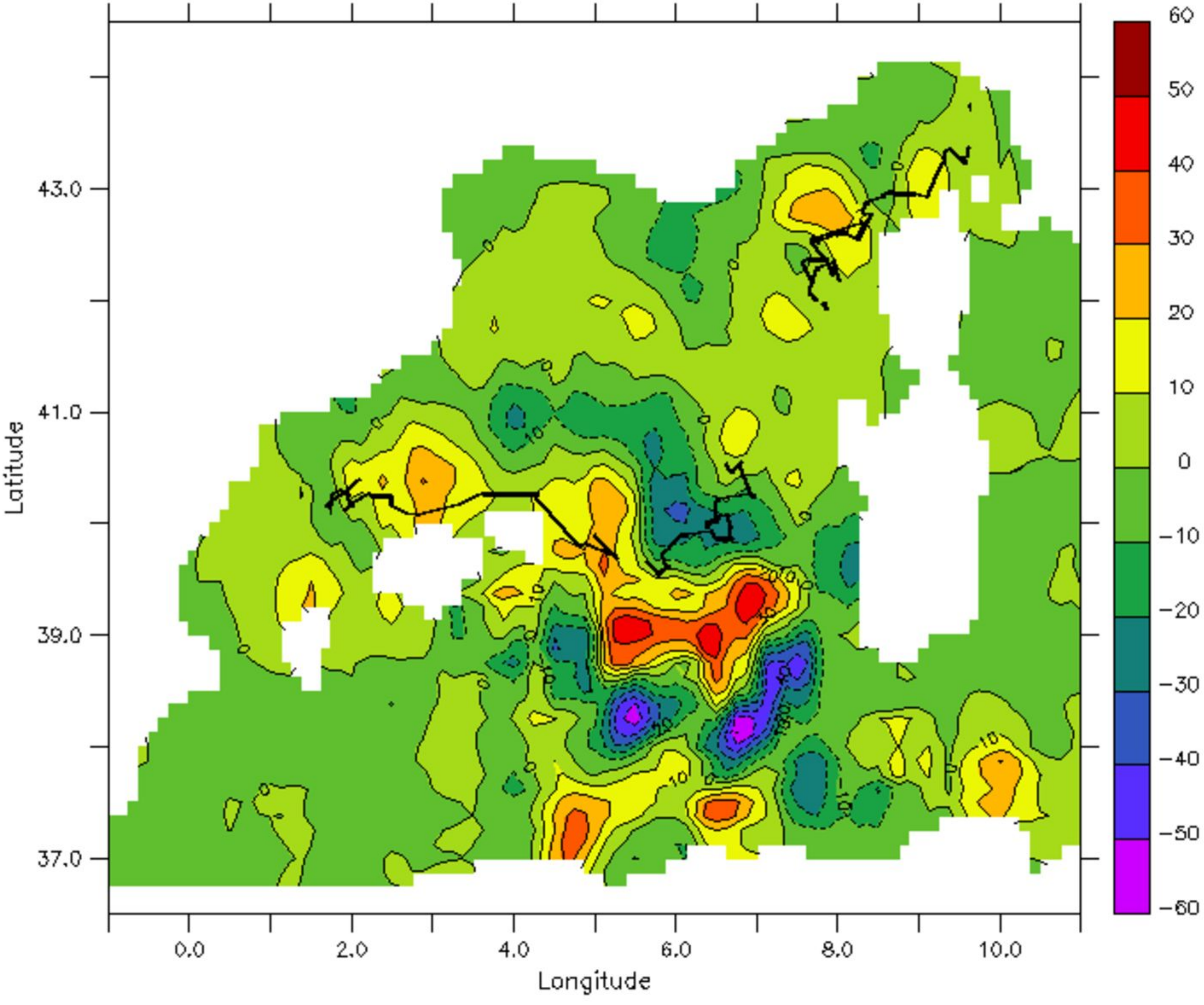
Latitude
Longitude
43.0
41.0
39.0
37.0
0.0
2.0
4.0
6.0
8.0
10.0
60
50
40
30
20
10
0
−10
−20
−30
−40
−50
−60
10
20
40
10
-10
-20
-40

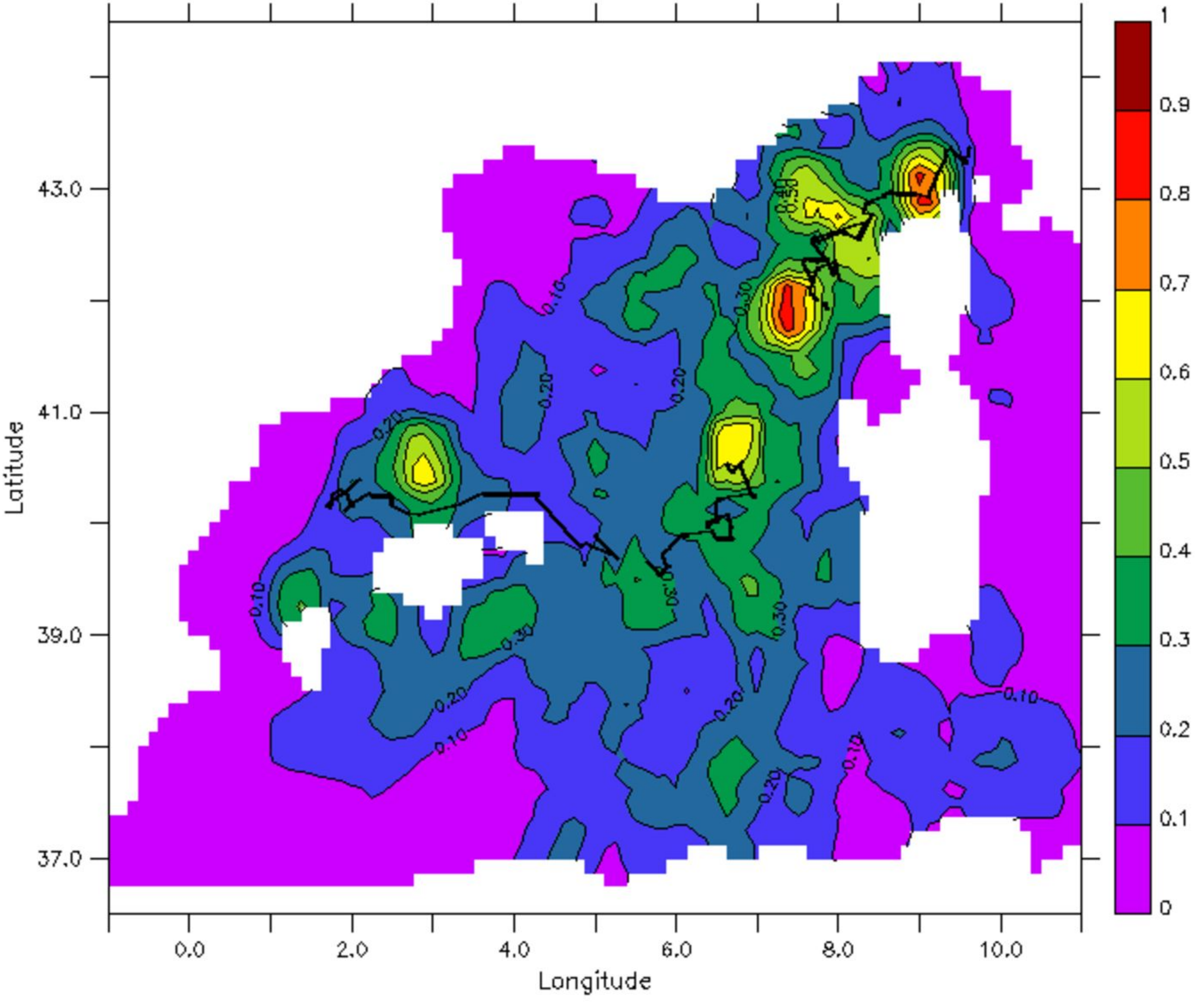
Latitude
43.0
41.0
39.0
37.0
Longitude
0.0
2.0
4.0
6.0
8.0
10.0
1
0.9
0.8
0.7
0.6
0.5
0.4
0.3
0.2
0.1
0
0.10
0.20
0.30
0.40
0.50

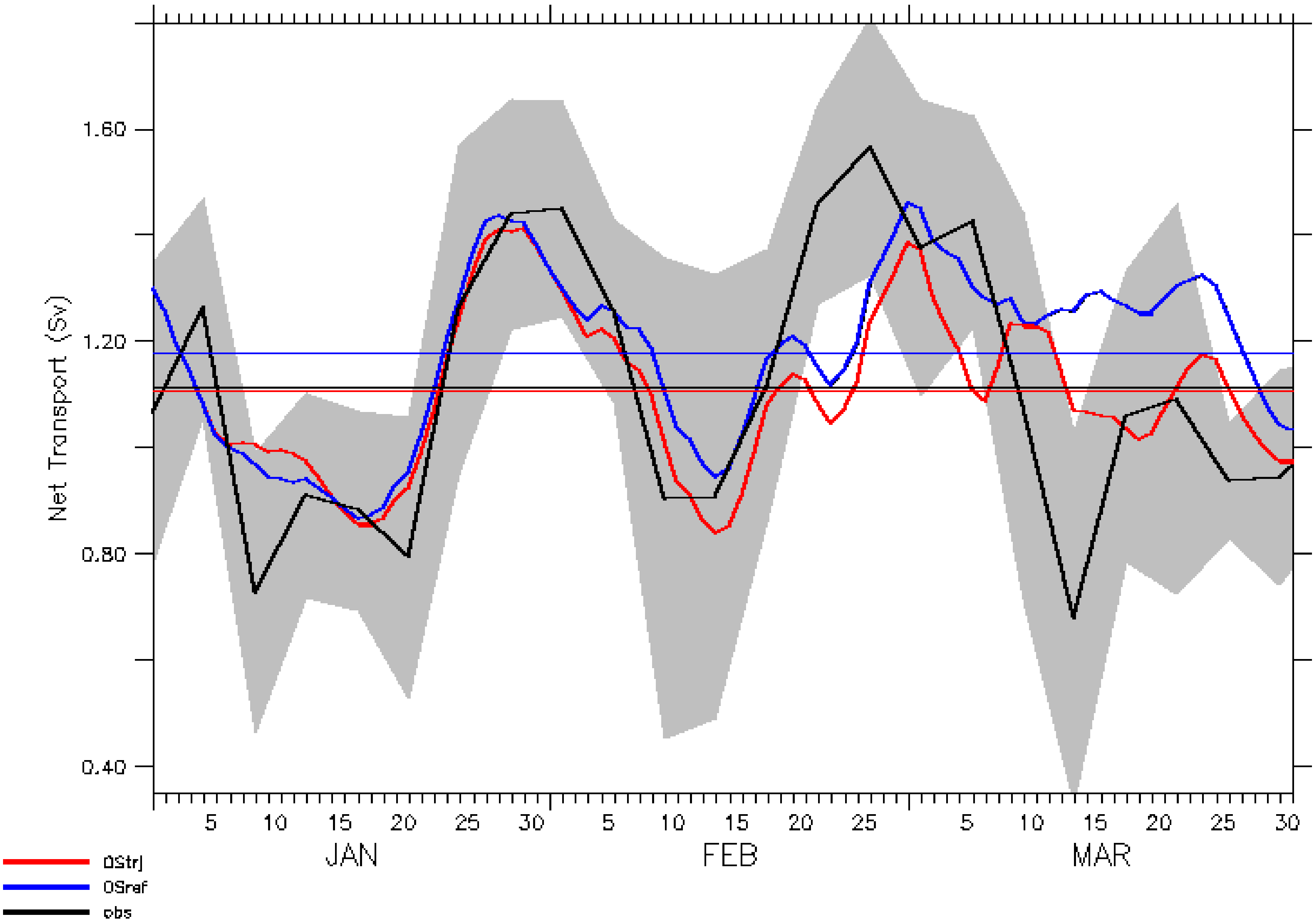
Net Transport (Sv)
1.60
1.20
0.80
0.40
5
10
15
20
25
30
5
10
15
20
25
5
10
15
20
25
30
JAN
FEB
MAR
OStrj
OSref
obs